JOURNAL OF GEOPHYSICAL RESEARCH, VOL. 98, NO. B5, PAGES 8275–8291, MAY 10, 1993

Deformation of the Oceanic Crust Between the North American and South American Plates

R. DIETMAR MÜLLER

Scripps Institution of Oceanography, La Jolla, California

WALTER H.F. SMITH[1]

Institute of Geophysics and Planetary Physics, Scripps Institution of Oceanography, La Jolla, California

Fracture zone trends and magnetic anomalies in the Atlantic Ocean indicate that the North American plate must have moved with respect to the South American plate during the opening of the Atlantic. A comparison of plate tectonic flow lines with fracture zones identified from Geosat and Seasat altimeter data suggests that the North American-South American plate boundary migrated northward from the Guinea–Demarara shear margin to the Vema Fracture Zone before chron 34 (84 Ma), to north of the Doldrums Fracture Zone before chron 22 (51.9 Ma), and to north of the Mercurius Fracture Zone between chron 32 (72.5 Ma) and chron 13 (35.5 Ma) . The paleoridge offset through time identified from magnetic anomalies and the computed cumulative strike slip motion in the plate boundary area, indicate that the triple junction may have been located between the Mercurius and the Fifteen-Twenty fracture zones after 67 Ma (chron 30). Plate reconstructions indicate a Late Cretaceous phase of transtension, followed by transpression in the Tertiary for the Tiburon/Barracuda Ridge area south of the Fifteen-Twenty Fracture Zone. The ocean floor in this area is characterized by a series of ridges and troughs with large Bouguer gravity anomalies (up to ~135 mGal). We use smoothing spline estimation to invert Bouguer anomalies for crustal layer structure. Our model results suggest that the Moho is uplifted 2-4 km over short wavelengths (~70 km) at the Barracuda and Tiburon ridges and imply large anelastic strains. The severely thinned crust at the two ridges implies that crustal extension must have taken place before they were uplifted. We propose that the North-South American plate boundary migrated to the latitude of the Tiburon Ridge, bounded by the Vema and Marathon fracture zones, before chron 34 (84 Ma). Post-chron 34 crustal thinning during a transtensional tectonic regime may have been localized at preexisting structural weaknesses such as the Vema, Marathon, Mercurius, and Fifteen-Twenty fracture zone troughs, but reaching the Fifteen-Twenty Fracture Zone and future Barracuda Ridge area only after chron 32 (72.5 Ma). This interpretation concurs with our crustal structural model, which shows stronger crustal thinning underneath the Tiburon Ridge than at the Barracuda Ridge. Subsequent transpression may have continued along the existing zones of weakness in the Tertiary, creating the presently observed crustal deformation and uplift of the Moho, accompanied by anelastic failure of the crust. Middle-Eocene-Upper Oligocene turbidites on the slope of the Tiburon Ridge, now located 800 m above the abyssal plain, suggest that most of its uplift occurred at post-Oligocene times. The unusually shallow Moho underneath the Tiburon and Barracuda ridges represents an unstable density distribution, which may indicate that compressive stresses are still present to maintain these anomalies, and that the North American-South American plate boundary may still be located in this area.

INTRODUCTION

A dense pattern of mostly medium to large offset fracture zones as well as a series of unusual ridges and troughs with large gravity anomalies is found in the region bounded by the Fifteen-Twenty Fracture Zone to the north and the Romanche Fracture Zone to the south (Figure 1), in this paper referred to as the equatorial Atlantic. One reason for the tectonic complexity of this area may be that it recorded the migration of the plate boundary between the North and South American plates. However, the tectonic history of this area is not well known due to the lack of identified magnetic anomalies.

It has been suggested by several authors [*Roest and Collette*, 1986; *Roest*, 1987; *Cande et al.*, 1988] that this plate boundary was located in the equatorial Atlantic for a significant time span between the Late Cretaceous and the Late Tertiary; this suggestion is based mainly on evidence from fracture zone trends. Rifting between Africa and South America south of the Guinea–Demarara margin started in the Early Cretaceous and the first NOAM–SOAM–African oceanic triple junction is thought to have formed at about 110 Ma (Late Albian–Early Cenomanian) along the Guinea–Demarara shear margin [*Mascle et al.*, 1988], as shown on a tentative reconstruction for 100 Ma (Figure 2). All fracture zones identified from satellite altimetry data older than about 100 Ma preserved on the African plate show North American–African spreading directions (Figure 2), confirming that the triple junction was located at the Guinea–Demarara shear margin at that time.

A comparison of tectonic flow lines computed from published plate models with the fracture zones in the equatorial North Atlantic shows that North American-African flow lines clearly mismatch all fracture zones south of the Fifteen-Twenty Fracture Zone younger than chron 13 (36 m.y.) (Figure 3*a*), and that the South Atlantic flow lines mismatch the fracture zone segments older than chron 5 (10 Ma) north of the Marathon Fracture Zone (Figure 3*b*). This means that the NOAM–SOAM plate boundary must have been located in the area bounded by the Marathon and Fifteen-Twenty fracture zones between chrons 13 and 5, and that it migrated northward from its initial position at the Guinea–Demarara shear margin to this area some time before chron 13.

South Atlantic flow lines are compatible with fracture zones south of the Kane and north of the Fifteen-Twenty fracture zone

[1]Now at Geosciences Laboratory, Ocean and Earth Sciences, National Ocean Service, NOAA, Rockville, Maryland.

Copyright 1993 by the American Geophysical Union.

Paper number 92JB02863.
0148-0227/93/92JB-02863$05.00

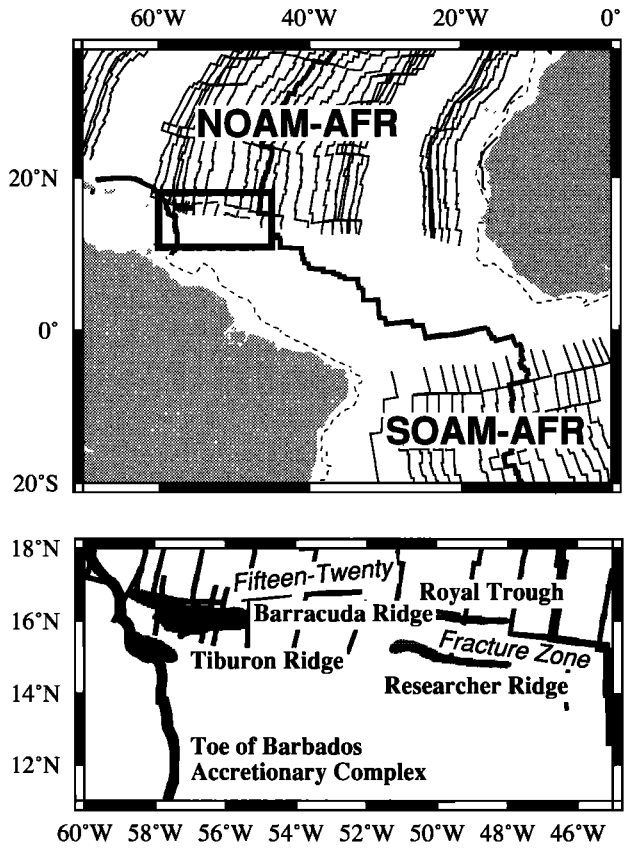

Fig. 1. (Top) Tectonic map of the central Atlantic Ocean. Heavy lines indicate identified plate boundaries (Mid-Atlantic Ridge, and the toe of the Barbados accretionary complex). Continental margins are dotted. Central North Atlantic and South Atlantic isochrons (shown as thin lines) formed by North American–African and South American–African plate motions. Central North Atlantic isochrons are constructed for chrons 5, 6, 13, 21, 25, 30, 32, 33y, 33o, 34, M-0, M-4, M-10N, M-16, M-21, M-25; South Atlantic isochrons are drawn for chrons 5, 6, 13, 18, 21, 25, 31, 34. Magnetic anomalies cannot be identified near the magnetic equator. (Bottom) Inset map showing anomalous ridge and trough features which we suggest were formed by tectonism at the North American–South American plate boundary. The Fifteen-Twenty Fracture Zone runs along the Barracuda Ridge and Royal Trough and meets the MAR at 15°20'N.

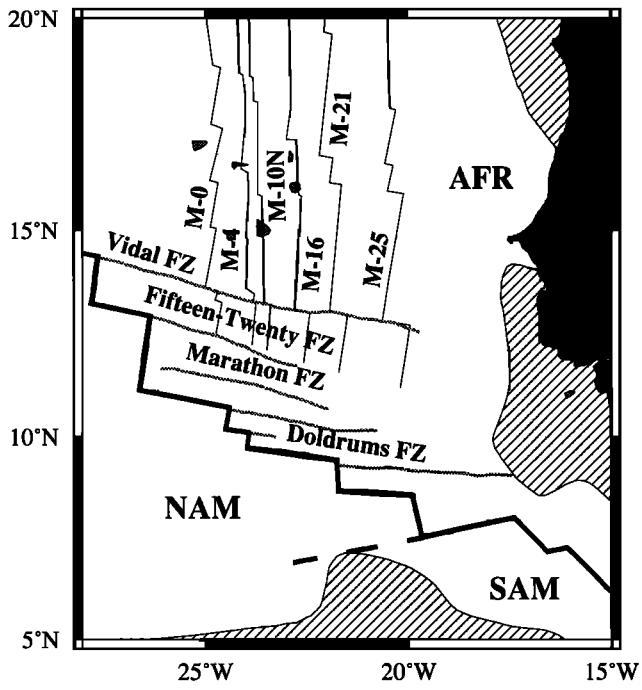

Fig. 2. Tentative reconstruction for 100 Ma, when rifting between Africa and South America south of the Guinea–Demarara margin had started. The first North–South American–African oceanic triple junction is thought to have formed at about 110 Ma (Late Albian–Early Cenomanian) along the Guinea–Demarara shear margin [*Mascle et al.*, 1988]. Evidence for the location of the NOAM–SOAM plate boundary at that time is provided by fracture zones older than about 100 Ma northwest of the Guinea Plateau, which show North American–African spreading directions.

only for the youngest stage (chron 5, 10 Ma, to present). This indicates that the NOAM–SOAM–African triple junction may have migrated to north of the Fifteen-Twenty Fracture Zone after chron 5.

Another bathymetric feature of this region in addition to the dense fracture zone pattern is a series of ridges and troughs in the vicinity of the Fifteen-Twenty Fracture Zone: the Barracuda Ridge and Trough, the Tiburon Ridge east of the Lesser Antilles Arc, and the Researcher Ridge and Royal Trough west of the Fifteen-Twenty transform fault (Figure 1). The Barracuda and Tiburon ridges exhibit unusually large gravity anomalies which may be indicative of plate boundary deformation processes. The Royal Trough exhibits en échelon shaped tectonic fabric and fresh basalts on a basement characterized by spreading center type faulting identified from GLORIA data, and the Researcher Ridge has a large magnetic anomaly; these are interpreted as extensional features [*Collette et al.*, 1984; *Roest and Collette*, 1986].

In this study we combine two approaches to better determine the history of the NOAM–SOAM plate boundary. First, we use combined Geosat ERM (44 stacked cycles) and Seasat along-track gravity data to obtain a more detailed image of fracture zone trends in the equatorial Atlantic and compare these with tectonic flow lines computed from published finite rotation poles, as summarized by *Müller and Roest* [1992]. We calculate estimates for the cumulative transpression/transtension along the plate boundary and compare the predicted strike slip component with reconstructed paleoridge offsets at the Fifteen-Twenty transform to better confine the time interval when the plate boundary may have been located in this area. Second, we combine ship and satellite gravity data with ship bathymetry data to model the crustal deformation underneath the Barracuda and Tiburon ridges by inversion of smoothed Bouguer anomalies for relief in a multilayer model of ocean crust.

SUMMARY OF PREVIOUS INVESTIGATIONS OF THE NOAM–SOAM PLATE BOUNDARY

The tectonic complexity of the equatorial Atlantic, in particular, the history and timing of the NOAM–SOAM plate boundary migration, has been the subject of controversy in the past. *Roest and Collette* [1986] suggested that the plate boundary migrated northward from south of 10° N to the Fifteen-Twenty Fracture Zone at about 10 Ma, creating the Barracuda Ridge and Trough by means of N-S compression in the vicinity of the North–South American rotation pole. Their model is based on a survey of the Fifteen-Twenty Fracture Zone between 30° and 60°W as well as mapped fossil spreading directions between the Fifteen-Twenty and the Vema fracture zones. *Roest* [1987] used Seasat altimetry data in the equatorial Atlantic for a comparison of tectonic flow lines with fracture zone gravity anomalies. He concluded that the North–

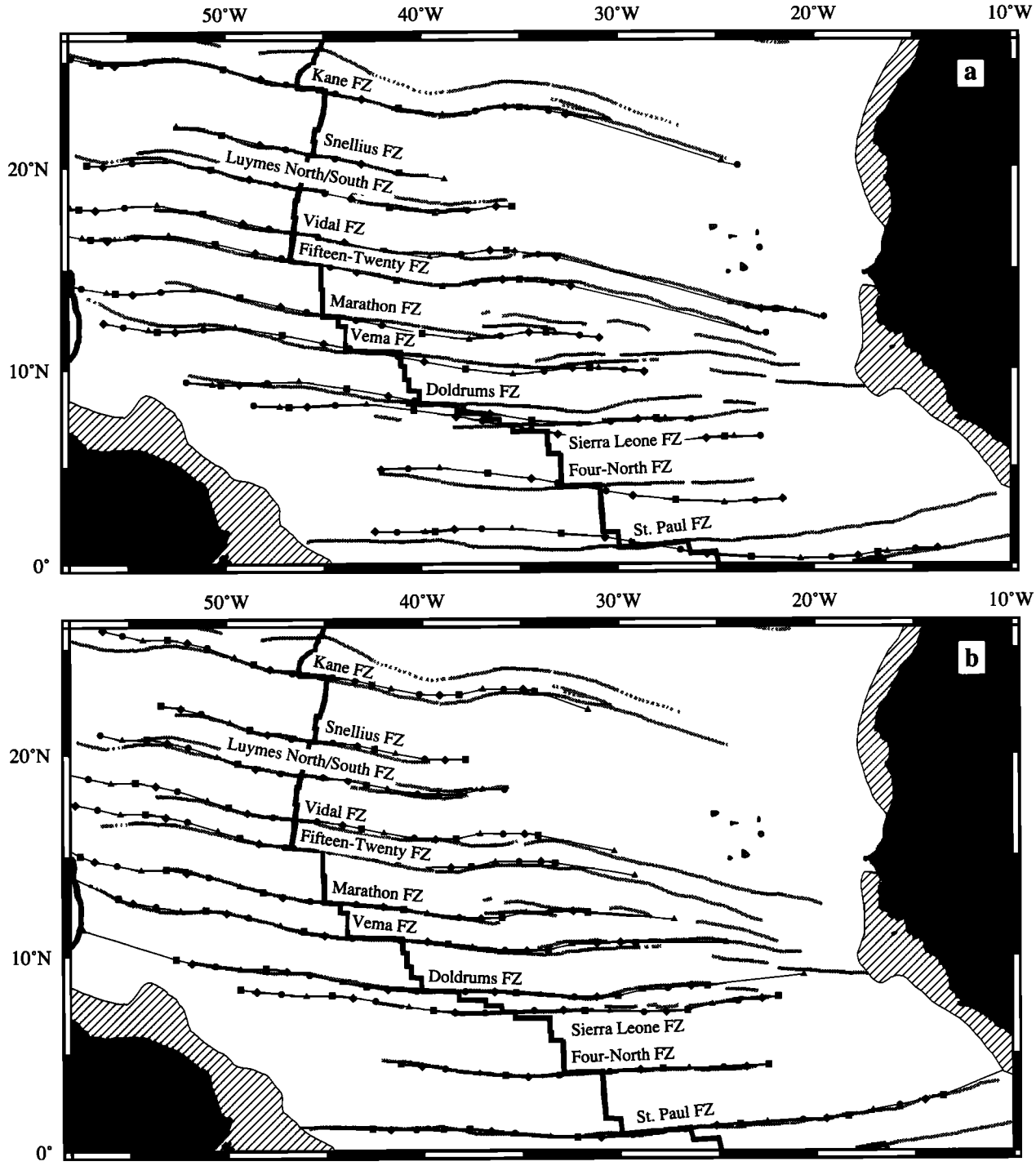

Fig. 3. Fracture zones identified from Geosat and Seasat altimetry data and plate tectonic flow lines from (*a*) North American-African stage poles and (see *Müller and Roest* [1992] for summary) and (*b*) from South American-African stage poles [*Shaw and Cande*, 1990]. Flow lines in Figure 3*a* are constructed for chrons 5 (10.0 Ma), 6 (20.0 Ma), 13 (35.5 Ma), 21 (49.5 Ma), 25 (59.0 Ma), 30 (67.5 Ma), 32 (72.5 Ma), 33y (74.3 Ma), 33o (80.2 Ma), 34 (84.0 Ma), M-0 (118.0 Ma), M-4 (126.0 Ma), M-10N (131.5 Ma), M-16 (141.5 Ma), M-21 (149.5 Ma), and M-25 (156.5 Ma); The South Atlantic flow lines in Figure 3*b* are computed for chrons 5 (8.9 Ma), 6 (19.4 Ma), 8 (26.9 Ma), 13 (35.3 Ma), 20 (44.7 Ma), 22 (51.9 Ma), 25 (58.6 Ma), 30 (66.7 Ma), 33y (74.3 Ma), 33o (80.2 Ma), 34 (84.o Ma) and 100 Ma (extrapolated from the stage 33o-34). See text for discussion. The central North Atlantic flow lines (a) mismatch all fracture zones south of the Sierra Leone Fracture Zone (SLFZ) for times younger than chron 34 (84 Ma) and mismatch all fracture zones south of the Fifteen-Twenty Fracture Zone (Fifteen-Twenty Fracture Zone) for times younger than chron 13 (36 Ma); the South Atlantic flow lines (b) clearly mismatch fracture zones north of the Fifteen-Twenty Fracture Zone. The North American-South American plate boundary must have been located in the area between the Fifteen-Twenty Fracture Zone and the SLFZ through most of the spreading history in this area. Hatchures indicate stretched continental crust.

South American plate boundary was located south of the Four North Fracture Zone between chrons 34 and 13 and subsequently migrated northward, passing the Doldrums Fracture Zone. *Roest* [1987] found that the Vema Fracture Zone shows the southern spreading directions since about 20 Ma, whereas the Mercurius, Marathon and Fifteen-Twenty Fracture Zones display the southern pattern since 10 Ma. *Cande et al.* [1988] also utilized Seasat altimetry data to interpret the location of fracture zones between the Fifteen-Twenty and North Doldrums fracture zones, which they compared with South and central North Atlantic flow lines. They found that the South Atlantic flow lines follow the trends of the Marathon, Vema, and Doldrums fracture zones as far back as chron 21 (50 Ma), although the North and South American flow line trends for times prior to chron 13 are relatively similar. Hence *Cande et al.* [1988] concluded that the NOAM–SOAM plate boundary had migrated northward (to the Fifteen-Twenty Fracture Zone) at least at chron 13 (35 Ma), but may have migrated north of the Marathon Fracture Zone as early as chron 21 (50 Ma).

FRACTURE ZONES

Data

We utilized combined Geosat and Seasat deflection of the vertical data (equivalent to along-track horizontal gravity anomalies) to obtain short-wavelength vertical gravity anomalies along-track by Hilbert transformation. We high-pass filtered the vertical gravity along-track with a Gaussian filter (σ=11.2 s, λ=400 km) to isolate wavelengths related to isostatically uncompensated short-wavelength fracture zone topography [*McKenzie and Bowin*, 1976; *Mulder and Collette*, 1984].

We identified small- and medium-offset fracture zones from the along-track Geosat and Seasat gravity data by picking the center of the gravity troughs corresponding to the deepest portion of the central fracture valleys. We chose this methodology because the topography of fracture zones formed in slowly spreading ocean crust is associated with large-amplitude (2-3 km) median valleys and a basement trough at the age offset [*Tucholke and Schouten*, 1988]. Also igneous rocks dredged from similar depths from the facing walls of fracture zones in slowly spreading ocean crust in the Indian Ocean differ in type, e.g. gabbros versus basalts, serpentinites versus basalts [*Engel and Fisher*, 1975], indicating a location of the fracture zone at the bottom of the central fracture valley. This contrasts with large-offset fracture zones in fast spreading ocean crust that exhibit a step morphology modulated by flexural topography from differential subsidence and thermal bending with a fracture zone location at the steepest slope of the geoid step [*Wessel and Haxby*, 1990]. *Müller et al.* [1991] showed that the average mismatch between the short-wavelength geoid trough and the basement trough of 37 profiles crossing the Kane Fracture Zone in the central North Atlantic is about 5 km, providing "ground truth" for using satellite altimetry data for identifying fracture zones in this area.

Large offset fracture zones (Romanche, St. Paul), which are mainly characterized by a depth-age step, were located by using the inflection point of the vertical gravity signal, corresponding to the steepest slope of the depth-age step. The interpreted fracture zones are shown on Figures 3 and 4. Flow lines for central North Atlantic (Figure 3*a*, 4*a*) and South Atlantic (Figure 3*b*, 4*b*) seafloor spreading were computed from recently published finite rotation poles (see *Müller and Roest* [1992] for a summary). All ages of magnetic anomalies referred to in the following are based on the time scale by *Kent and Gradstein* [1986].

Comparison Between Fracture Zones and Synthetic Flow Lines

In order to use the dense fracture zones between the Marathon and Sierra Leone fracture zones for obtaining evidence about the plate boundary migration we have plotted both South-American-African (Figure 4*a*) and North American-African flow lines (Figure 4*b*) for comparison with fracture zone trends. Figure 3 illustrates that North American-African flow lines clearly mismatch fracture zones south of the Fifteen-Twenty Fracture Zone for times after chron 13 (35.5 Ma). As a result, the parts of these flow lines older than chron 13 are virtually meaningless because they have been so far offset from the fracture zones that they are meant to model (Figure 3*a*). In order to utilize the older North American-African flow line information, we have used South American-African flow lines as shown in Figure 4a to obtain the correct flow line positions at chron 13. We used these positions as new "seed points" to compute North American-African flow lines for times older than chron 13.

The Marathon Fracture Zone reflects South Atlantic spreading from chron 20 to present day (Figure 4*a*). The fracture zones between the Mercurius and the Sierra Leone fracture zones are fairly consistent with the South Atlantic spreading directions back to about chron 34 (Figure 4*a*). However, many North American-African flow lines for times between chron 13 (35.5 Ma) and chron 32 (72.5 Ma) also give a reasonable fit to these fracture zones (Figure 4*b*). Therefore it appears that the northward migration of the NOAM–SOAM plate boundary to north of the Mercurius Fracture Zone must have occurred after chron 32 and before chron 13.

There are four densely spaced fracture zones south of the Doldrums Fracture Zone (Figure 3) that are highly segmented and cannot be traced as far back as the fracture zones to the north. For post-chron 22 (51.9 Ma) times the South Atlantic flow lines match the trends of these fracture zones quite well, while the trend of central North Atlantic flow lines clearly mismatches these fracture zones. This demonstrates that the triple junction migrated to north of the Doldrums Fracture Zone some time before chron 22.

South Atlantic flow lines for the Cretaceous Magnetic Quiet Zone (chron M-0 (118.7 Ma) to chron 34 (84 Ma)) do not match the observed fracture zones south of the Vema Fracture Zone, but match the Vema and Marathon fracture zones reasonably well (Figure 4*a*). This indicates that the triple junction was located between the Guinea–Demarara shear margin and the Vema Fracture Zone from its initiation to chron 34.

A region of ocean crust older than chron M-0 (118.7 Ma) west of the Guinea Plateau is located east of the termination of the South Atlantic flow lines (Figure 4*a*), and the few fracture zone segments interpreted in this area fit central North Atlantic flow lines (Figure 4*b*). Clearly, this portion of ocean crust was created at the central North Atlantic ridge before the onset of South American-African spreading.

In summary, the interpreted fracture zone trends in the equatorial Atlantic are consistent with a northward migration from the Guinea–Demarara shear margin to the Vema Fracture Zone before chron 34 (84Ma), to north of the Doldrums Fracture Zone before chron 22 (51.9 Ma), and to north of the Mercurius Fracture Zone between chron 32 (72.5 Ma) and chron 13 (35.5 Ma).

TRANSPRESSION/TRANSTENSION ALONG THE NOAM–SOAM PLATE BOUNDARY

The area between the Fifteen-Twenty and Marathon fracture zones appears to be a likely candidate for plate boundary deformation, because it is accompanied by the Barracuda Ridge and

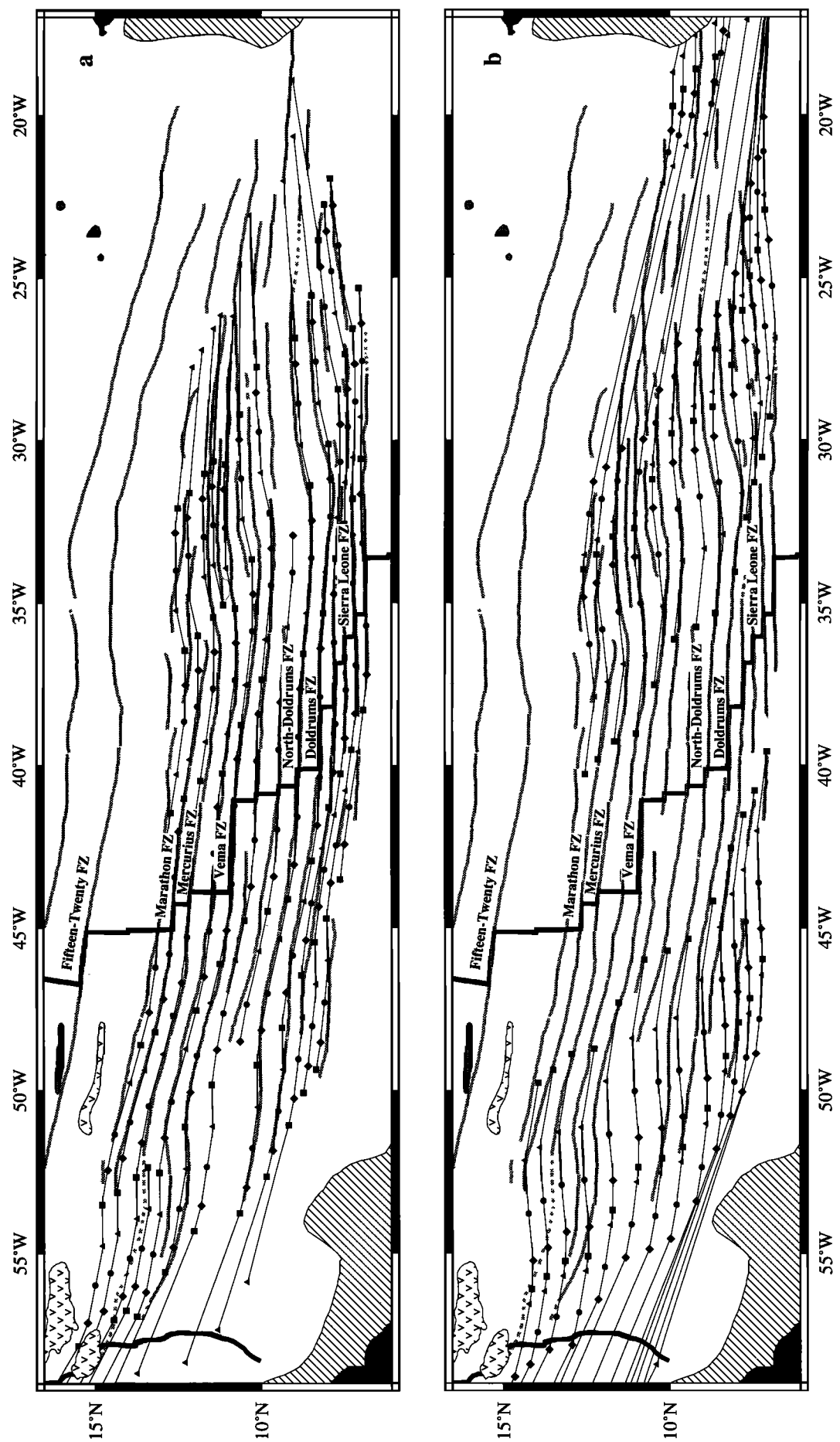

Fig. 4. Comparison of fracture zones with synthetic (*a*) South American-African and (*b*) North American-African flow lines in the equatorial Atlantic. Flow lines are constructed for the same times as in Figure 3. The interpreted fracture zone trends in the equatorial Atlantic are consistent with a northward migration from the Guinea–Demarara shear margin to the Vema Fracture Zone before chron 34 (84 Ma), to north of the Doldrums Fracture Zone before chron 22 (51.9 Ma), and to north of the Mercurius Fracture Zone between chron 32 (72.5 Ma) and chron 13 (35.5 Ma). See text for discussion.

Trough and the Tiburon Ridge as well as the Researcher Ridge and Royal Trough west of the present-day Fifteen-Twenty Transform Fault. All these bathymetric features show elements of plate boundary deformation, either compressional or extensional [*Roest and Collette*, 1986]. Following our fracture zone analysis, we start with the working hypothesis that this area may have been the location of the plate boundary after chron 13 (35.5 Ma), and possibly before that time.

We can test the hypothesis that the plate boundary may in fact have been located at the Fifteen-Twenty Fracture Zone by calculating the strike slip motion along the NOAM–SOAM plate boundary at this fracture zone through time and comparing it with the reconstructed offsets of the Fifteen-Twenty Fracture Zone. If this hypothesis is correct, the present-day offsets of magnetic anomalies north and south of the fracture zone would reflect the cumulative differential strike slip along various portions of the plate boundary.

Only a few magnetic anomalies in the equatorial Atlantic south of the Fifteen-Twenty Fracture Zone have been identified because of the location of this roughly east-west spreading area at the magnetic equator, where inclination approaches zero. The magnetic anomaly picks identified in this area are from *Klitgord and Schouten* [1986]. If we reconstruct the relative position of the magnetic picks north and south of the Fifteen-Twenty Fracture Zone by using the North American–African and South American–African rotation parameters, respectively, we obtain the paleo-offset of the Mid-Atlantic Ridge at the triple junction through time. We test our working hypothesis by plotting the paleo-ridge offset against the cumulative strike slip motion through time (Figure 5), calculated from the finite rotation poles in Tables 1*a* and 1*b*.

The reconstructed offset of the Fifteen-Twenty Fracture Zone increases from 95 to 145 km from chron 34 (84 Ma) to chron 32 (72.5 Ma). The predicted strike slip for the same time is 115 km, over twice as much as the observed offset of magnetic lineations at the fracture zone that varies between 25 and 50 km. This discrepancy is most readily explained by the inference that the plate

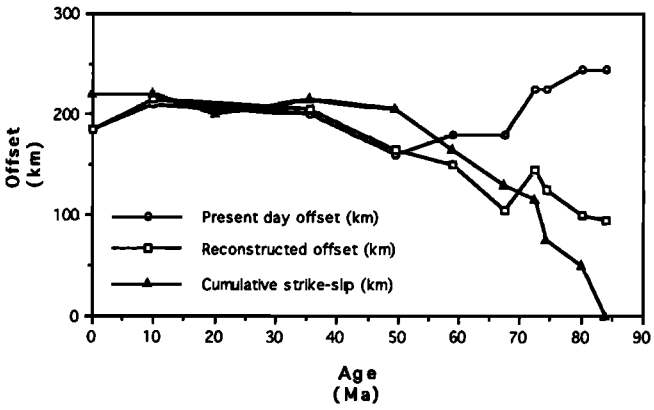

Fig. 5. The paleoridge offset versus the cumulative strike-slip motion at the Fifteen-Twenty Fracture Zone yields strong evidence that the plate boundary was located here from chron 30 (67.5 Ma) to chron 5 (10 Ma). For times after chron 33o (80.2 Ma) there is a good agreement between 45 km of total increase in fracture zone offset and 65 km of predicted strike-slip from chron 33o to chron 32 (72.5 Ma). Between chron 32 and 30 (67.5 Ma) the fracture zone offset is reduced from 145 to 105 km, although the plate model predicts continued left-lateral strike-slip of 15 km, probably reflecting a ridge jump. In the following time (chron 30 to chron 5 (10 Ma)) the fracture zone offset increases from 105 to 215 km until chron 5, in good agreement with 90 km of predicted cumulative strike slip.

TABLE 1*a*. North–South American Finite Reconstruction Poles

Anomaly	Age, Ma	Latitude, °N	Longitude, °E	Angle, deg.
5	10.4	17.2	-53.5	2.00
6	20.5	15.1	-54.1	3.91
13	35.5	16.7	-53.7	5.72
21	50.3	15.5	-53.8	7.12
25	58.6	13.8	-52.0	8.31
31	68.5	12.2	-53.4	9.50
34	84.0	6.4	-58.0	9.31

North–South American finite reconstruction poles and stage poles. Calculated from the rotation poles summarized by *Müller and Roest* [1992]. A positive rotation angle indicates counterclockwise rotation.

TABLE 1*b*. North–South American Stage Poles for North America

Age 1, Ma	Age 2, Ma	Latitude, °N	Longitude, °E	Angle, deg.
0.0	10.4	17.2	-53.5	-2.00
10.4	20.5	12.9	-54.6	-1.91
20.5	35.5	20.2	-53.0	-1.82
35.5	50.3	10.6	-53.9	-1.41
50.3	58.6	4.4	-41.2	-1.23
58.6	68.5	0.5	-61.7	-1.23
68.5	84.0	-57.1	-147.8	-1.22

See Table 1*a* footnotes.

boundary was not located at the Fifteen-Twenty Fracture Zone during the entire time interval but migrated to this location some time after chron 32.

Between chron 32 and 30 (67.5 Ma) the fracture zone offset is reduced from 145 to 105 km, although the plate model predicts continued left-lateral strike slip of 15 km. This observation may reflect a ridge jump in response to the continued lateral separation of the two ridge segments bounding the fracture zone. In the following time (chron 30 to chron 5 (10 Ma)) the fracture zone offset increases from 105 to 215 km until chron 5, while 90 km of cumulative strike slip are predicted. Hence for this period there is an excellent agreement between the predicted strike slip and observed increase in offset, yielding evidence that the plate boundary may have been located at the Fifteen-Twenty Fracture Zone from chron 30 to chron 5. However, we point out that a direct correlation between observed changes in offset and predicted strike slip cannot be expected, because transform offsets also change in response to changes in direction of plate motion.

To further test whether the plate boundary may have been located in the Fifteen-Twenty Fracture Zone area, we now compute the cumulative compression/extension along this fracture zone by using the central North Atlantic and the South Atlantic rotation parameters. Two phases of differing tectonic regimes can be distinguished for the differential motion history along the plate boundary. From chron 33o to 30 the entire plate boundary from crust as old as 84 Ma to the mid-ocean ridge was subjected to left-lateral transtension, resulting in up to ~50 km extension in the area of the western Barracuda Ridge. After chron 30 the tectonic regime changed to transpression along the entire plate boundary. At chron 21 (49 Ma), transtension replaced transpression along the eastern portion of the plate boundary. Since we rely on published reconstructions for computing the differential motion along the plate boundary, we restrict ourselves to computing the cumulative compression and extension for post-chron 30 times. The calculated total deformation from chron 30 to chron 5 along the plate boundary amounts to 70 km of compression in the western Barracuda Ridge area, 30 km of compression in the eastern Barracuda Ridge area, and about 30 km of extension in the Researcher Ridge–Royal Trough area, if the plate boundary was in fact located at the Fifteen-Twenty Fracture Zone during this time (Figure 6).

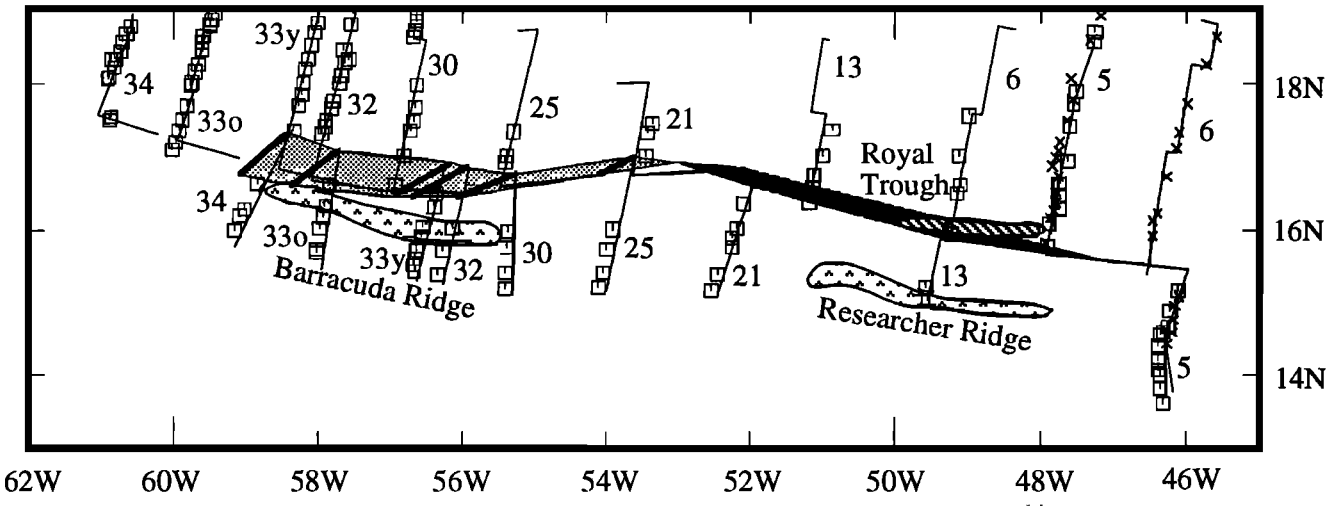

Fig. 6. Magnetic anomaly picks from North and South America (open squares), and anomaly picks rotated from Africa (crosses) in a reconstruction for chron 5 (10 Ma). Fracture zone (FZ) picks from NOAM and SOAM are solid squares; FZ picks rotated from Africa are solid triangles. Light gray area near Barracuda Ridge indicates cumulative transpression from chron 30 (67.5 Ma) to chron 5. Dark gray area near Royal Trough indicates cumulative transtension from chron 21 (49 Ma) to chron 5. The calculated total deformation from chron 30 to chron 5 along the plate boundary amounts to 70 km of compression in the western BR area, 30 km of compression in the eastern BR area, and 30 km of extension in the RT, if the plate boundary was in fact located in this area.

Roest and Collette [1986] speculated that both the topography and the gravity anomaly of the Barracuda Ridge indicate compression at a time when the lithosphere had gained considerable thickness. However, they could not clearly distinguish between compressional and extensional deformation from seismic profiles across the Barracuda Trough. Seismic data from the sediments in the trough south of the Barracuda Ridge and from the Tiburon Ridge (*Peter and Westbrook*, 1976; *Mascle and Moore*, 1990) show widespread normal faults but few reverse faults. Therefore these seismic reflection data do not seem to provide unequivocal evidence for the style of tectonic deformation in this area.

The computed transtension east of anomaly 21 coincides with the occurrence of the Researcher Ridge and Royal Trough, which *Roest and Collette* [1986] interpreted as a constructional volcanic ridge and extensional basin, respectively. The eastern termination of the Researcher Ridge is located west of anomaly 6. Transtension younger than chron 6 apparently did not cause constructional volcanism, but resulted in formation of the Royal Trough. The absence of any volcanic ridge east of the Researcher Ridge and the presence of the Royal Trough to the north may indicate that some time between chrons 6 and 5 the plate boundary jumped to north of the Fifteen-Twenty Fracture Zone.

TOPOGRAPHY AND GRAVITY ANOMALIES

Data

If the NOAM–SOAM plate boundary had been located in the Fifteen-Twenty Fracture Zone area and the ocean floor in that area were subject to initial transtension and subsequent transpression, we might expect to find evidence for crustal deformation. Here we examine bathymetry and gravity anomalies for clues to crustal deformation. The western equatorial Atlantic is relatively densely covered by ship tracks (Figure 7). We combine ship and satellite free-air gravity data with ship bathymetry data to construct gridded topography and gravity data sets (Figures 8*a* and 8*b*). Both data types are gridded at 2.5 arc min of latitude and longitude using continuous curvature splines in tension [*Smith and Wessel*, 1990]. Because ship gravity data have DC offsets [*Wessel and Watts*, 1988], we adjusted the DC level of each ship to match the satellite gravity field prepared from combined Seasat, Geosat, and ERS–1 altimeter data [*Sandwell and Smith*, 1992]. For each ship survey, we form the difference between the ship and satellite data and adjust the ship data so that the mean difference becomes zero. The adjusted differences are then gridded and added to the satellite data to form the gravity field shown in Figure 8. The accuracy of the ship bathymetry data was assessed by *Smith* [1993].

The topography and gravity data in Figure 8 are strongly anticorrelated in the southwest corner of the maps, near Barbados. The topography rises to shallow levels on the Barbados accretionary complex; the gravity shows large negative values, presumably because the depth to the Moho is increasing on the subducting plate. We find that this anticorrelation produced spurious trends in our gravity modeling, and therefore we detrend the gravity and topography data. Trends are computed by gridding the data in a larger area than shown in Figure 8, and using a 400-km median filter over the observed data grids to define the trend (Figure 8*c* and 8*d*). The trends are essentially "flat" over much of the map area outside the accretionary wedge, and so the detrending makes little change (other than mean level) in the data in this area. The detrended data are shown as Figure 8*e* and 8*f*.

The largest gravity anomalies in the western equatorial Atlantic are associated with the Barracuda and the Tiburon ridges (Figures 8*a* and 8*e*). The Barracuda Ridge has a clear topographic expression (Figure 8*b* and 8*f*); the Tiburon Ridge is not easily defined topographically because of its proximity to the Barbados accretionary complex but appears as a distinct structural high in seismic reflection profiles [*Mauffret et al.*, 1984].

Bouguer Gravity Anomalies

We obtain the Bouguer gravity anomaly grid shown in Figure 9 by removing the gravity effect of the detrended topography (Figure

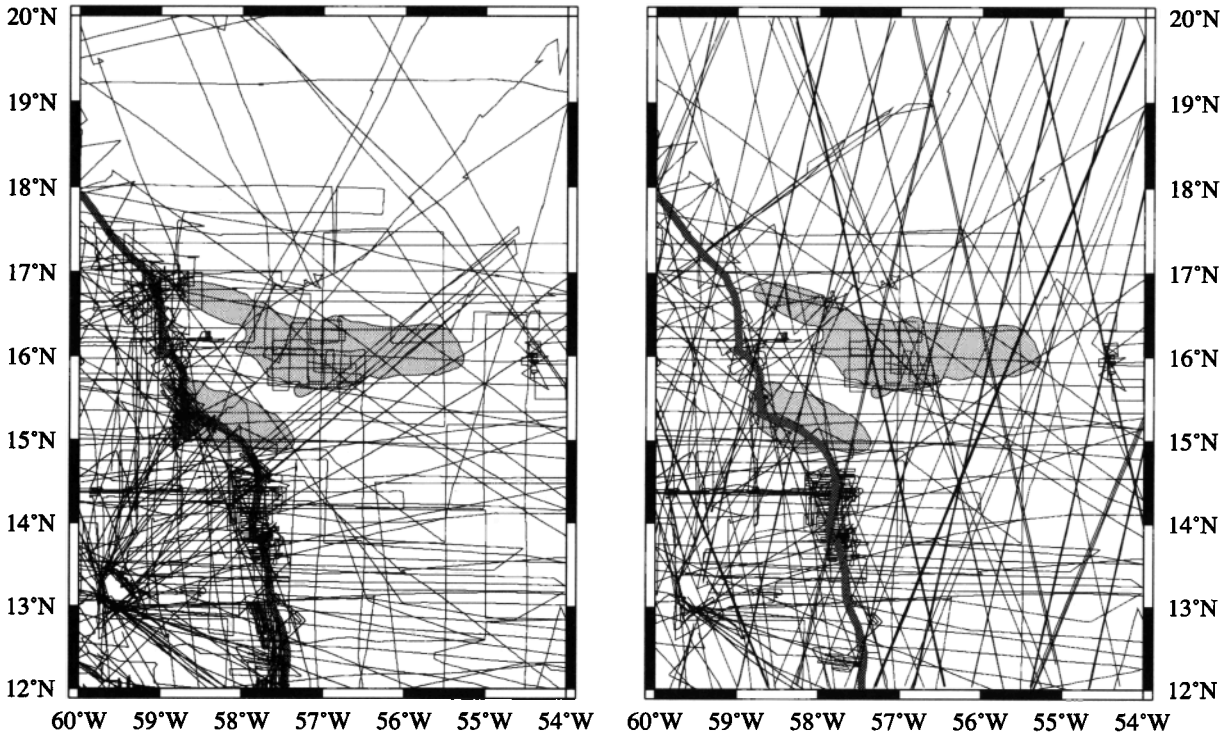

Fig. 7. (*a*) Ship bathymetry tracks and (*b*) gravity tracks from ship and satellite altimetry data in the western equatorial Atlantic. The Barracuda and Tiburon ridges (Figure 1) are indicated by the gray areas.

8*f*) from the detrended gravity (Figure 8*e*), assuming a density of 2800 kg m^{-3} for the topography. In this calculation, we use *Parker's* [1972] expression for the gravity effect of a density contrast $\Delta\rho$ with a varying elevation h(x), x is a 2-vector indicating a position in the plane:

$$F[g(\mathbf{x})] = 2\pi G\,\Delta\rho\, exp(-|\mathbf{k}|\,z) \sum_{n=1}^{\infty} \frac{|\mathbf{k}|^{n-1}}{n!} F[(h(\mathbf{x}))^n]. \quad (1)$$

Here F [] indicates a Fourier transform, g(x) is the predicted gravity anomaly, G is Newton's gravitational constant, **k** is a Fourier wave vector ($k_x = 2\pi/\lambda_x$, $k_y = 2\pi/\lambda_y$, where λ is a wavelength), and z is the mean depth to the density contrast (5200 m for the seafloor topography). We took four terms in the series (1).

Bouguer gravity anomalies are usually negative over positive elevations of the seafloor, because these are isostatically compensated. The opposite is true at the Barracuda Ridge, where the Bouguer gravity reaches +100 mGal. Immediately to the north in the Barracuda Trough, the Bouguer gravity is negative (-60 mGal) while the bathymetry is flat. The largest positive Bouguer anomaly (135 mGal) is over the Tiburon Ridge. This feature is at the limit of the area affected by detrending. South of the Tiburon Ridge there is another negative Bouguer anomaly (-80 mGal), indicating another trough.

Inversion of Bouguer Anomalies for Layered Structure

Bouguer anomalies indicate changes in crustal thickness or density, or vertical displacement of structural contacts in a (normally) horizontally layered crust (e.g., layer 2, layer 3, Moho). Most models of marine gravity anomalies are constructed using a layered oceanic crust [cf. *Watts*, 1978]. Gravity interpretation is nonunique, and any number of structures can be devised which will fit the observed gravity anomaly. If we assume that the Bouguer anomaly shown in Figure 9 is caused by undulations of a density contrast at the Moho, then equation (1) can be used to calculate the Bouguer gravity anomaly, g, given the Moho elevation, h, and the mean depth to the Moho, z.

If we attempt to invert the Bouguer gravity anomaly for the topography of the Moho surface, we have two difficulties: Equation (1) is nonlinear in h, and its inverse also involves downward continuation, which is unstable. It is convenient to separate these two difficulties by defining m, the Bouguer anomaly at the mean depth of the Moho:

$$m(\mathbf{k}) = 2\pi G\,\Delta\rho \sum_{n=1}^{\infty} \frac{|\mathbf{k}|^{n-1}}{n!} F[(h(\mathbf{x}))^n]. \quad (2)$$

Equation (2) is a nonlinear problem for h, given m, which can be solved by iterative approximation [*Oldenburg*, 1974]. Substitution of (2) into (1) gives

Fig. 8. We combined ship and satellite free-air gravity data with ship bathymetry data to construct gridded topography and gravity data sets (Figures 8*a* and 8*b*). The topography and gravity data are strongly anticorrelated in the southwest corner of the maps, near Barbados. We found that this anticorrelation produced spurious trends in our gravity modeling, and so we detrended the gravity and topography data. Trends were computed by gridding the data in a larger area than shown and using a 400-km median filter over the observed data grids to define the trend (Figures 8*c* and 8*d*). The trends are essentially "flat" over much of the map area outside the accretionary wedge, and so the detrending makes little change (other than mean level) in the data in this area. The detrended data are shown as Figures 8*e* and 8*f*.

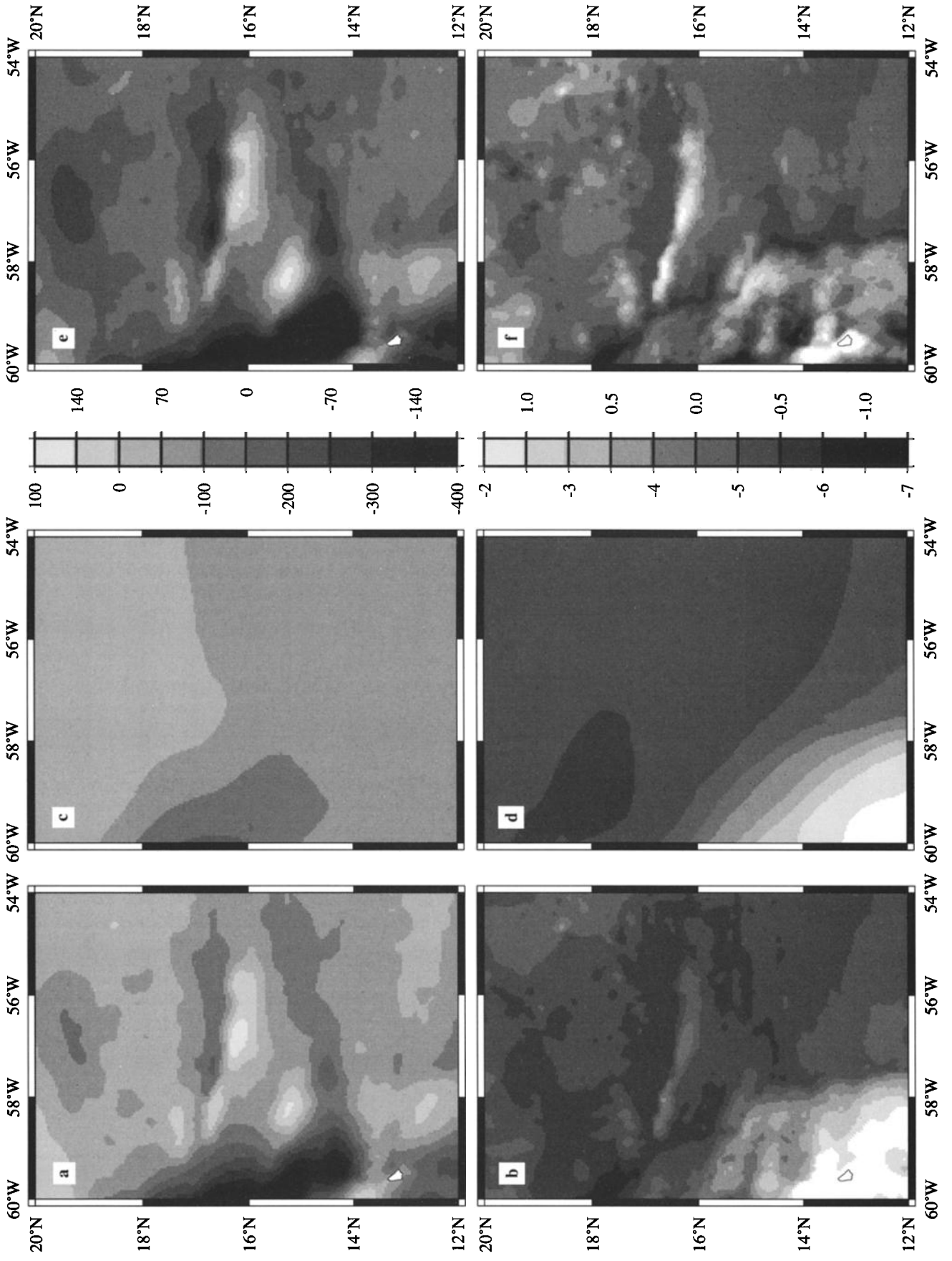
a
b
c
d
e
f
60°W
58°W
56°W
54°W
20°N
18°N
16°N
14°N
12°N
100
0
-100
-200
-300
-400
-2
-3
-4
-5
-6
-7
140
70
0
-70
-140
1.0
0.5
0.0
-0.5
-1.0

$$g(\mathbf{k}) = exp[-|\mathbf{k}|\, z]\; m(\mathbf{k}) \tag{3}$$

which is the unstable inverse problem of downward continuation of g to obtain m.

Stable estimates of m may be obtained from (3) by low-pass filtering of g before downward continuation. We use a filter which minimizes the curvature of m, because the curvature of h is indicative of deformation in the crust. Estimation of a minimum-curvature m from noisy g is similar to the problem of deconvolution by smoothing spline estimation [*Constable and Parker*, 1991]. *Morgan and Blackman* [Inversion for crustal structure from combined gravity and bathymetry data: a prescription for downward continuation, subm. to J. of Geophys. Res.] suggested a similar approach for modeling the Moho at mid-ocean ridges. Let the estimated Bouguer gravity anomaly at the Moho level be $\hat{m}$. Then the integrated squared curvature of $\hat{m}$. is

$$L = \iint |\mathbf{k}|^4\, [\hat{m}(\mathbf{k})]^2\, d\mathbf{k} \tag{4}$$

and the integrated squared misfit of $\hat{m}$. to the data g is

$$E = \iint [g(\mathbf{k}) - exp[-|\mathbf{k}|\, z]\; \hat{m}(\mathbf{k})]^2\, d\mathbf{k} \tag{5}$$

Now we may choose $\hat{m}$. so as to minimize the sum

$$E + \nu L \tag{6}$$

where ν is a parameter that adjusts the relative weight of E and L. As $\nu \to 0$, $\hat{m}$ will fit g exactly, while as $\nu \to \infty$, $\hat{m} \to 0$. Some intermediate choice of ν produces a smooth $\hat{m}$ with a reasonable fit to the data. The estimate $\hat{m}$ which minimizes the sum (6), given ν, is

$$\hat{m}(\mathbf{k}) = g(\mathbf{k}) \left[\frac{exp[-|\mathbf{k}|\, z]}{exp[-2|\mathbf{k}|\, z] + \nu |\mathbf{k}|^4} \right]. \tag{7}$$

Equation (7) is a filter that is applied to g to obtain $\hat{m}$. Because ν has units of k^{-4}, it is convenient to define a characteristic wavelength λ of the filter (7) as

$$\lambda = 2\pi \nu^{1/4}. \tag{8}$$

In Figure 10a, we show the root-mean-square (RMS) misfit (in milliGals), as a function of λ (in kilometers). The RMS is found by dividing $E^{1/2}$ by the number of grid elements.

We obtained $\hat{m}$ for the values of λ shown in Figure 10a and inverted (2) for the Moho elevation h in each case. We then computed the absolute value of the curvature of the Moho elevation, $|\nabla^2 h|$, to assess the extent of crustal deformation implied by $\hat{m}$. Curvatures up to approximately 10^{-6} m^{-1} can be sustained by elastic flexure of the ocean lithosphere, while curvatures exceeding this value are expected to result in failure [*McNutt*, 1984]. At crustal levels, this failure is expected to take place by brittle faulting. Figure 10b shows the percent of the map area of Figure 9 over which the Moho curvatures exceed the elastic limit, for various values of the parameter λ.

Figure 10 is an illustration of the classic trade-off between resolution and variance [*Backus and Gilbert*, 1970; *Menke*, 1989]. If we choose a small value for λ, we fit the data very well, but the model implies a Moho which is faulted nearly everywhere;

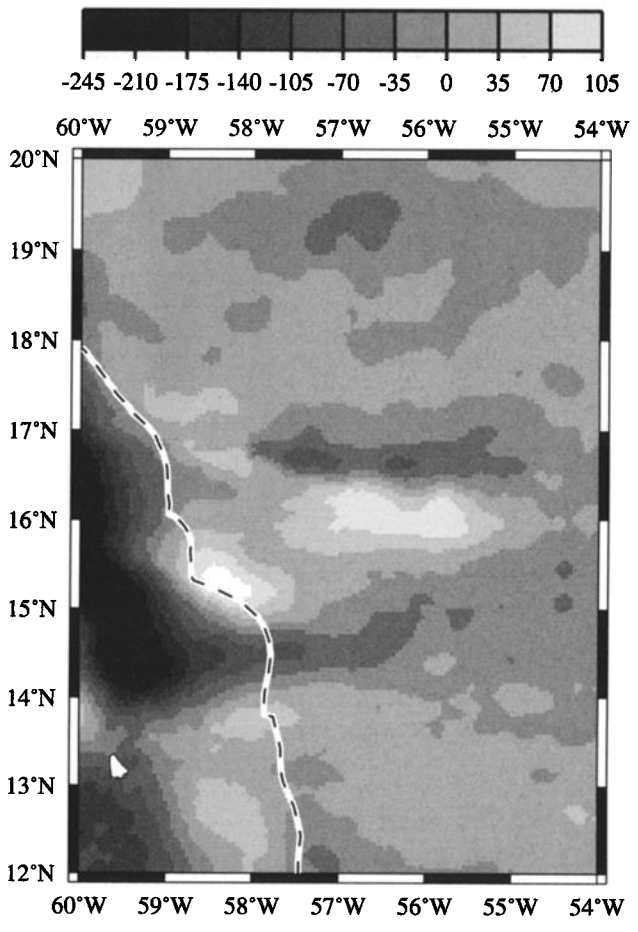

Fig. 9. Bouguer gravity anomalies in the western equatorial Atlantic. Note the positive Bouguer anomalies at the Barracuda Ridge (up to 100 mGal), and at the Tiburon Ridge (up to 135 mGal). Negative Bouguer anomalies are found in the Barracuda Trough (-60 mGal) and the South of the Tiburon Ridge (-80 mGal), indicating another trough.

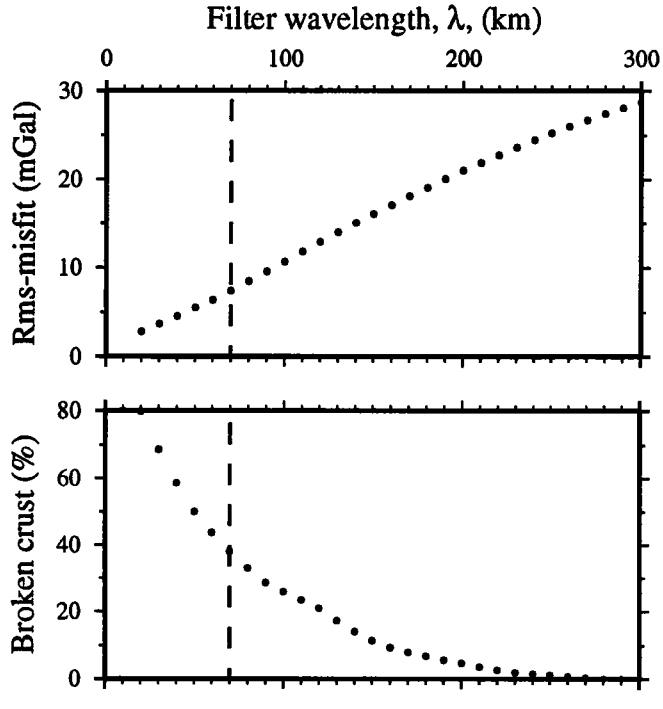

Fig. 10. Root mean square misfit and percent of faulted crustal area versus wavelength of the smoothing spline filter, showing the classic trade-off between resolution and variance. If we choose a small value for l, we fit the data very well, but the model implies a moho which is faulted nearly everywhere; conversely, a large value of l yields a model with a mostly unbroken Moho but a poor fit to the data.

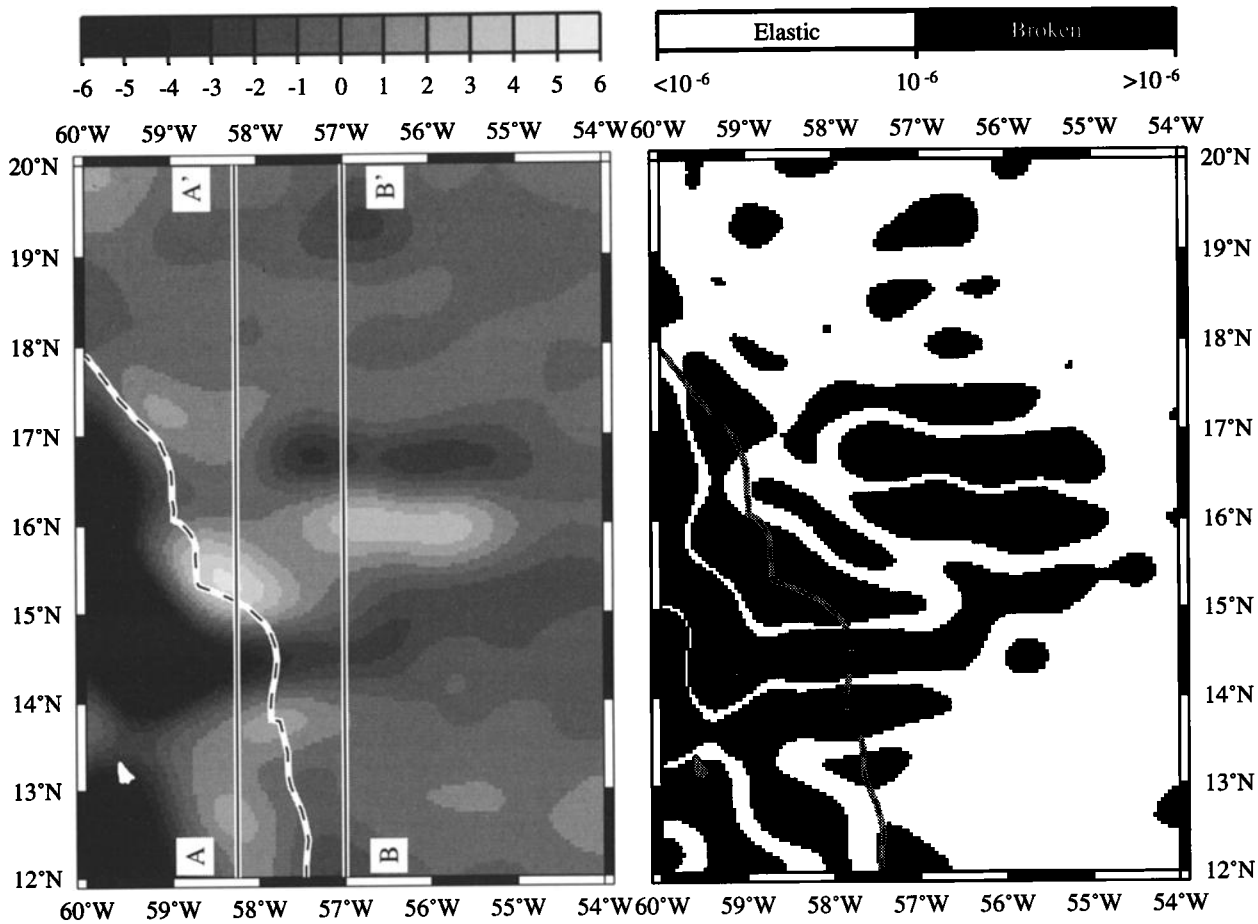

Fig. 11. (*a*) Moho elevation and (*b*) distribution of elastic failure from the l = 70 km model with a density contrast of ρ_m–ρ_c (ρ_m=3300 kg m^{-3}, ρ_c=2800 kg m^{-3}). The Moho is elevated underneath the ridges and deflected downward under the adjacent troughs, resulting in severe crustal thinning and thickening reflecting the large positive and negative Bouguer gravity anomalies over the ridges and troughs (Figure 11*a*). The modeled Moho shows large curvatures in the area of the Tiburon and Barracuda ridges and troughs as well as in the Barbados accretionary prism, while curvatures larger than 10^{-6} are less common outside of these areas (Figure 11*b*).

conversely, a large value of λ yields a model with a mostly unbroken Moho but a poor fit to the data. There is no obvious choice of λ from Figure 10. We chose λ based on two criteria: First it is our expectation that large Moho curvatures should be generally confined to the area of the Tiburon and Barracuda ridges and troughs and the subduction zone complex, where the large Bouguer gravity anomalies are observed. Second is our desire that the model should fit the gravity anomaly data as well as possible at the Tiburon and Barracuda ridges and troughs. Using these criteria, we chose λ = 70 km.

Figure 11a shows the Moho elevation and Figure 11b the distribution of elastic failure from the λ = 70 km model with a density contrast of ρ_m–ρ_c (ρ_m=3300 kg m^{-3}, ρ_c=2800 kg m^{-3}). The modeled Moho shows large curvatures in the area of the Tiburon and Barracuda ridges and troughs as well as in the Barbados accretionary prism, while curvatures larger than 10^{-6} are less common outside of these areas (Figure 11b). The modeled Moho west of the toe of the accretionary complex, shown as a dashed line in Figures 11a and 11b, is not relevant for our objectives and cannot be interpreted, because we detrend the data in this area. Cross-sectional profiles through the model at the Tiburon Ridge (A–A') and the Barracuda Ridge and Trough (B–B') are shown in Figure 12. The Moho is elevated underneath the ridges and deflected downward under the adjacent troughs, resulting in severe crustal thinning and thickening, reflecting the large positive and negative Bouguer gravity anomalies over the ridges and troughs.

The smoothing-spline model results in a fairly good fit of the model-gravity anomalies to the observed gravity anomalies (Figure 12) with an RMS misfit of 7.4 mGal. Although the one-layer crustal model satisfies the observed gravity field well, it is does not provide us with a realistic model for the crustal structure, because it does not consider the large variations in sediment thickness in this area. Published seismic profiles [*Peter and Westbrook*, 1976; *Mauffret et al.*, 1984] show deep sediment-filled troughs bordering the Barracuda and Tiburon ridges. The density we use for inverting the Bouguer anomalies is too large in our 1-layer model is too large, because sediments are less dense than upper crustal rocks. Consequently, we overestimate the amplitude and curvature of the modeled Moho underneath these troughs by using crustal densities.

In order to construct a more realistic model, we designed a nonlinear inversion method that considers sediments, as well as an upper crustal and a lower crustal layer. In this model we iteratively perturb initially flat-lying crustal layers by using smoothed residual gravity anomalies. These are smoothed using the spline filter (equation 7) with z = 5200 m to downward continue the residual

gravity to the mean seafloor depth. We use the densities and layer thicknesses given in Table 2 for the layered model, which are constrained by regional seismic data. Since we do not have enough seismic data to construct a complete sediment thickness map for our model area, we start our model with a sediment layer of 500 m thickness. This is a reasonable value for the average sediment thickness in this area, which varies between 100 and about 1000 m, except for even larger sediment thicknesses in the Barracuda Trough and the trough south of the Tiburon Ridge [*Tucholke et al.*, 1982].

In the multilayer model, we compute a residual anomaly grid from the Bouguer gravity anomalies by setting all gravity anomaly values smaller than 7.5 mGal to zero. We chose this value, because gravity cross-over errors show uncertainties of this order [*Wessel and Watts*, 1988]. We use the residual gravity anomalies to perturb all crustal layers in concert. By downward continuing to the sediment-water interface only, we perturb the crustal layers too little at each model step, but create a stable, converging inversion process. We create a layer perturbation p(x) from the smoothed residual gravity s(x) given by

$$p(\mathbf{x}) = s(\mathbf{x}) / 2\pi G(\rho_m - \rho_s) \quad (9)$$

where we use the entire density contrast in the layered model ($\rho_m - \rho_s$), because the perturbation will be added to all layers. Hence the layers maintain their thickness, except that we have to satisfy the constraint that no layer may rise above the seafloor. While a negative smoothed residual $s(\mathbf{x})$ will drive all subseafloor horizons down, with a sediment layer growing thicker as seismic layer two is depressed, a positive $s(\mathbf{x})$ will drive contacts up until they are truncated against the seafloor, which may expose deeper levels of the section.

Using the new perturbed crustal layer structure, we compute a new gravity model from (1) by summing the contributions from each density contrast in the layer structure. We compute the maximum absolute gravity residual as the observed minus the new model. Now we again compute a residual anomaly grid by setting all values smaller than 7.5 mGal to zero and smooth it by using the smoothing spline filter (7). We stop the model iterations, if the maximum absolute value of the smoothed residual gravity anomalies is smaller than 5 mGal. This is equivalent to using the Chebychev norm as convergence criterion.

The difference between the linear model using only one crustal layer and the multilayer model to invert residual gravity anomalies for Moho topography is illustrated in Figure 13. We designed a synthetic gravity anomaly with a positive and a negative peak (Figure 13) to show the effect of inversion for layer topography using the single-layer (Figure 13a) and the multilayer model (Figure 13b). The single-layer model results in a symmetric ridge/trough Moho topography (Figure 13a), whereas the inversion for multilayer topography results in an asymmetric layer structure with a large-amplitude ridge, underneath which layer 2 and parts of layer 3 are missing, and a smaller-amplitude trough, resulting from modeling the sediment fill in the trough.

TABLE 2. Thicknesses and Densities of Layers Used in Model

Layer	Thickness, m	Density, kg/m^3
Water column	5200	1030
Sediments	500 [a]	2300
Layer 2	2300 [b]	2800 [c]
Layer 3	4700 [b]	2950 [c]
Mantle		3400 [d]

[a] Mean undisturbed sediment thickness around the Barracuda Ridge from *Tucholke et al.* [1982].
[b] *Purdy* [1983].
[c] *Carlson and Herrick* [1990].
[d] *Watts* [1978].

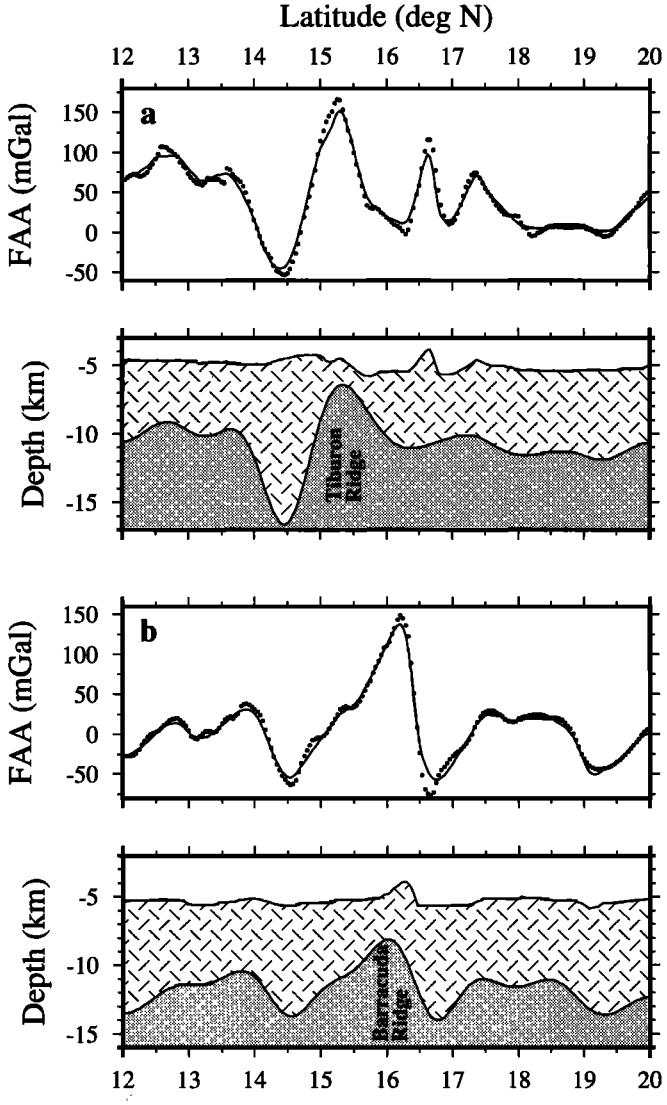

Fig. 12. Cross-sectional profiles through the crustal single-layer model at the Tiburon Ridge (A–A' on Figure 11) and the Barracuda Ridge and Trough (B–B' on Figure 11). The Moho is elevated underneath the ridges and deflected downward under the adjacent troughs, resulting in severe crustal thinning and thickening reflecting the large positive and negative Bouguer gravity anomalies over the ridges and troughs. Although the one-layer crustal model satisfies the observed gravity field well, it is does not provide us with a realistic model for the crustal structure, because it does not consider the large variations in sediment thickness in this area.

The Moho elevation (Figure 14a) and the distribution of elastic failure (Figure 14b) from the multilayer model is not drastically different from the single-layer model results (Figure 11). However, although we have used the same wavelength (70 km) for the smoothing filter in both models, we have created smoother Moho topography underneath the sediment-filled troughs in the multilayer model. This is reflected in the total area of elastic Moho failure, which is 30% in the multilayer model, as opposed to 38% in the single-layer model. Figure 15 shows two model cross sections over the Barracuda and Tiburon ridges and troughs. Comparison with Figure 12 reveals that the elevated Moho topography underneath the Barracuda and Tiburon ridges, resulting from positive residual gravity anomalies, is quite similar in both models.

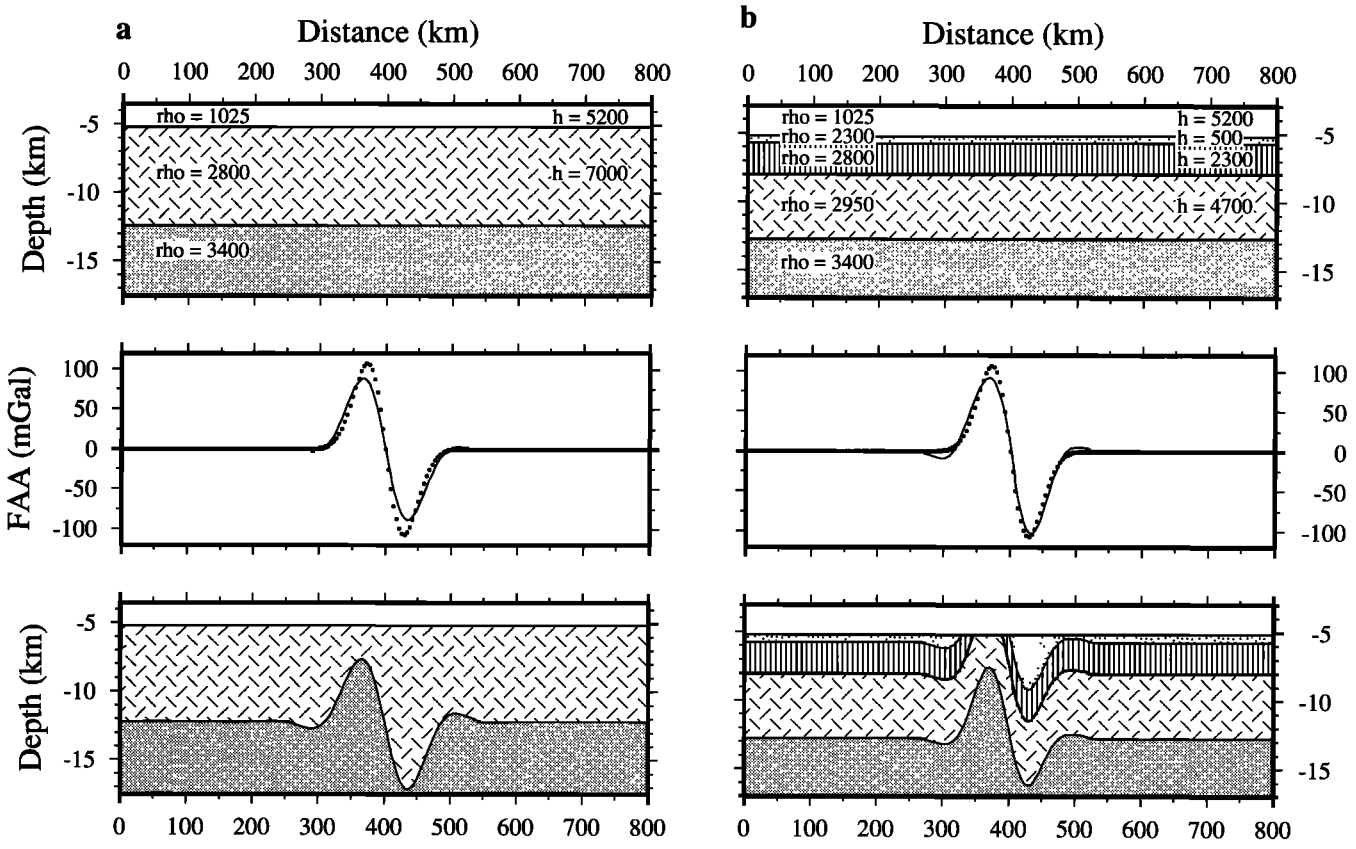

Fig. 13. Illustration of the perturbation of initially flat-lying layers by residual gravity anomalies using (*a*) the single-layer and (*b*) the multilayer model. The single-layer model results in a symmetric ridge/trough Moho topography (Figure 13*a*), whereas the inversion for multilayer topography results in an asymmetric layer structure with a large amplitude ridge, underneath which layer 2 and parts of layer 3 are missing, and a smaller-amplitude trough, resulting from modeling the sediment fill in the trough.

However, the layer structure modeled from large negative residual gravity anomalies, as over sediment-filled troughs south of the Tiburon Ridge and on both sides of the Barracuda Ridge, is smoother than in the single-layer model, resulting in a more realistic Moho curvature.

In order to check our model against seismic data from our study area, we show a cross section interpreted from a single-channel seismic profile by *Mauffret et al.* [1984] that crosses the Tiburon and western Barracuda ridges (Figure 16a), and compare it with our modeled layer structure sampled along this ship-track (Figure 16b). Note that the seismic section has a vertical axis in two-way travel time, while the model section is in kilometers. Both profiles show a deep sediment filled trough north of the Barracuda Ridge and outcropping basement at the Tiburon Ridge. The top of the Barracuda Ridge in our model section appears to consist of sediment (Figure 16b). This is a result of inverting smoothed residual gravity anomalies. We start our model with a 500m thick sediment layer, and use smoothed residual gravity anomalies ($\lambda >$ 70km) to perturb the layer structure. Topographic ridges of widths smaller than 35 km may remain covered with sediment, because short-wavelength gravity anomalies that may accompany these features are not inverted for layer structure.

DISCUSSION

It is important to bear in mind the nonuniqueness of gravity interpretation when examining the crustal sections in Figures 12 and 15. Layered models are convenient to calculate, but they may not always be appropriate. For example, thinning of layer three is observed at fracture zones [*Detrick et al.*, 1982; *Sinha and Louden*, 1983] and has been invoked to explain the Blake Spur Fracture Zone gravity anomaly [*Morris et. al.*, 1991], although this anomaly is an order of magnitude smaller than the anomaly over the Barracuda Ridge. Since the formation of the Barracuda Ridge and Trough seems related to the Fifteen-Twenty Fracture Zone, it might be appropriate to draw a model with a thinned layer 3 along the Barracuda Ridge/Trough. However, because this area has undergone an episode of extension, followed by compression, we really have no idea what sort of crustal section is reasonable. The displacement of subseafloor layers shown in Figures 12 and 15 need not be thought of as representing the actual configuration of the crust; they may be interpreted as merely a proxy for changes in density or thickness as well as layer displacement. For example, uplift of the Moho may be seen as indicative of increased density; this increase need not actually occur by Moho uplift. Nevertheless, there is independent evidence for uplift of material from deep structural levels at the Barracuda Ridge: mantle peridotites have been dredged from the Fifteen-Twenty Fracture Zone during cruises of the Soviet research vessel *Boris Petrov* in 1989 and 1990 [J. Casey, pers. communication, 1991].

Compressional deformation by elastic buckling has been invoked to explain gravity anomalies in the Indian Ocean [*Karner and Weissel*, 1990]. This is not appropriate for the gravity anomalies studied here. A topographic compensation mechanism for the

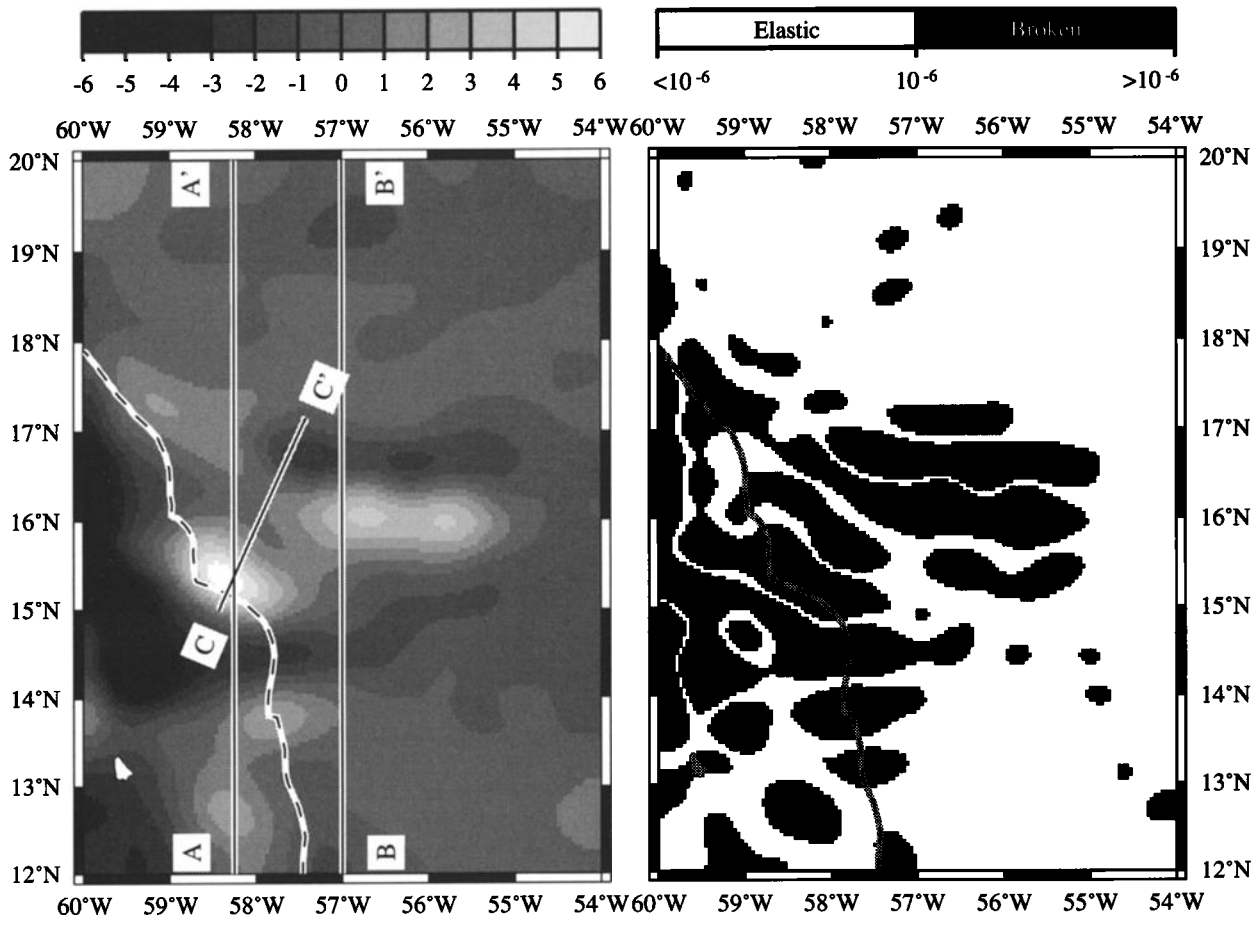

Fig. 14. (*a*) Moho elevation and (*b*) the distribution of elastic failure from the multilayer model. We have used the same wavelength (70 km) for the smoothing spline filter as in the single-layer model but have created smoother Moho topography underneath the sediment filled troughs in the multilayer model. This is reflected in the total area of elastic Moho failure, which is 30% in the multilayer model, compared with 38% in the single-layer model.

Barracuda and Tiburon ridges can be excluded, for they are uncompensated. We have also shown that elastic buckling cannot account for the crustal structure of the ridges and troughs, because the large, short-wavelength Bouguer gravity anomalies require curvatures exceed the elastic limit of about 10^{-6} m^{-1} [*McNutt*, 1984]. Our inversion procedure yields smoothly undulating contacts which resemble geological folds. Although we cannot directly describe faults in our models, the large curvatures of these contacts suggest that the crust underneath the anomalous ridges and troughs in this area is broken and faulted. Deep seismic reflection data from this area are not available to us to test this inference. Shallow reflection profiles show a prevalence of normal faults in sediments south of the Barracuda Ridge and on the Tiburon Ridge [*Peter and Westbrook*, 1976; *Mascle and Moore*, 1990]. In the Barracuda Trough seismic data show disturbed sediments but do not allow a distinction between normal and reverse faults [*Roest and Collette*, 1986].

We calculate the north–south crustal shortening along our multilayer model profiles A–A' and B–B' over the 900-km length of the profiles. The shortening we obtain is of the order of 500 m, that is negligible. This is a result of the smoothing in our inversion method. In contrast, a maximum shortening of 30-70 km at the Barracuda Ridge is calculated from plate kinematic models (Figure 6). It is unlikely that the shortening predicted from the plate reconstructions is grossly in error. The central North Atlantic and the South Atlantic are among the oceanic regions best covered by magnetic anomaly and fracture zone data. Even if the kinematic shortening were more than 50% less, of the order of 10-20 km, we would still be left with an order of magnitude more than that resolved by gravity inversion. Hence the inversions performed here are not a good method for estimating strain. Because the plate kinematic analysis suggests large shortening and the Moho curvatures under the ridges exceed the elastic limit, we believe that large strains are localized in these areas. *Zuber and Parmentier* [1991] have made a careful analysis of the compressional deformation of the ocean lithosphere. They find that once strain exceeds the linear elastic limit, a runaway instability occurs which rapidly localizes large strains. Such a process may describe what we see at these ridges.

However, the question remains how the cumulative North American-South American transtension and transpression calculated from plate kinematic models may be reconciled with the crustal structure modeled from gravity inversion. In summary, plate kinematic modeling, inversion of gravity anomalies, and geological/geophysical data from the study area include the following model results and observations:

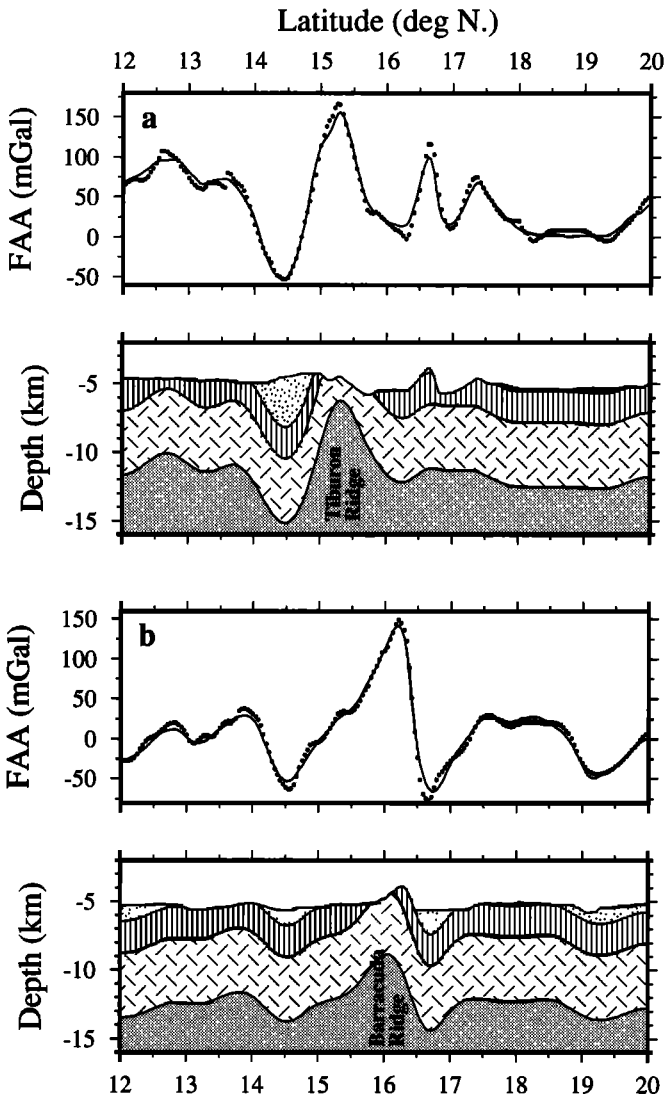

Fig. 15. Cross-sectional profiles from the multilayer model at the same locations as shown in Figure 12. Comparison with Figure 12 reveals that the elevated Moho topography underneath the Barracuda and Tiburon ridges, resulting from positive residual gravity anomalies, is quite similar in both models. However, the layer structure modeled from large negative residual gravity anomalies, as over sediment-filled troughs south of the Tiburon Ridge and on both sides of the Barracuda Ridge, is smoother than in the single-layer model, resulting in a more realistic Moho curvature.

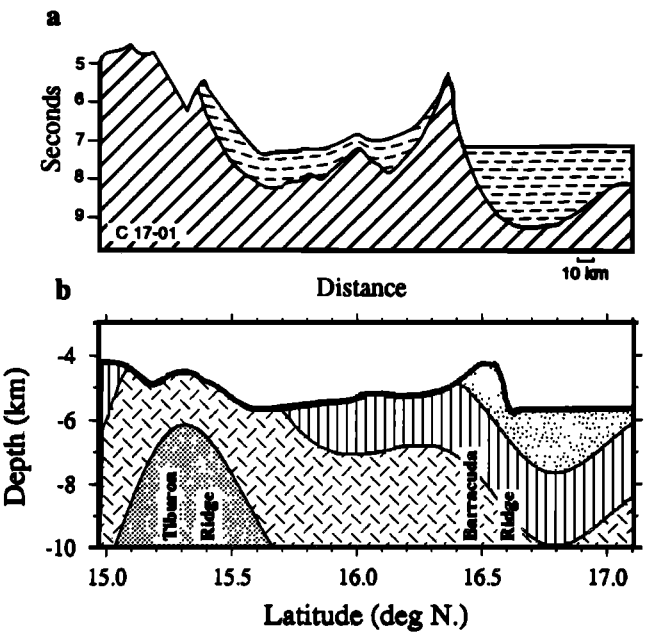

Fig. 16. (*a*) Comparison of a seismic profile from *Mauffret et al.* [1984] that crosses the Tiburon and western Barracuda ridges (C-C' in Figure 14) (*b*) with our modeled layer structure sampled along the same track. Note that the seismic section has a vertical axis in two-way travel time, while the model section is in kilometers. Both profiles show a deep sediment-filled trough north of the Barracuda Ridge and outcropping basement at the Tiburon Ridge. The top of the Barracuda Ridge in our model section appears to consist of sediment. This is a result of inverting smoothed residual gravity anomalies. We start our model with a 500 m-thick sediment layer and use smoothed residual gravity anomalies ($l > 70$ km) to perturb the layer structure. Topographic ridges of widths smaller than 35 km may remain covered with sediment, because short-wavelength gravity anomalies that may accompany these features are not inverted for layer structure.

1. The North American-South American plate boundary was initiated at the Guinea-Demarara shear margin in the Late Cretaceous. A comparison of fracture zones with synthetic plate flow lines shows that it migrated to the area between the Marathon and Fifteen-Twenty fracture zones, where the Barracuda and Tiburon ridges are located, some time between chron 32 (72.5 Ma) and chron 13 (35.5 Ma).

2. Differential motion between North America and South America calculated for the Barracuda Ridge area from plate kinematic data suggests a phase of left-lateral transtension between chron 34 (84 Ma) and 30 (67.0 Ma) that would have resulted in over 100 km of strike slip and ~50 km extension. However, a large discrepancy between the change in offset of the Fifteen-Twenty Fracture Zone with the predicted strike slip during that time suggests that the plate boundary was more likely located south of the Fifteen-Twenty Fracture Zone/Barracuda Ridge during this time. Between chron 30 (67 Ma) to chron 5 (10 Ma) right-lateral transpression is predicted from plate kinematics for the Barracuda Ridge area, with 90 km of cumulative strike slip, and 30-70 km of compression.

3. The Barracuda Trough is coincident with the western extension of the Fifteen-Twenty Fracture Zone [*Roest and Collette*, 1986]. The deep trough south of the Tiburon Ridge may be bounded by the western extensions of the Mercurius and Vema Fracture Zones (Figure 4).

4. The large gravity anomaly over the Tiburon Ridge requires a crustal thickness of only 1.5-2 km, indicating a very shallow Moho (Figure 15a). The Moho depth underneath the Barracuda Ridge is modeled to be 4 km below seafloor (Figure 15b). In both cases layer 2 is inferred to be absent; underneath the Tiburon Ridge, even the thickness of layer 3 is reduced considerably. This indicates severe crustal thinning along these uncompensated ridges and active Moho uplift. Sediment filled troughs several kilometers deep are found adjacent to the ridges

5. Moho curvatures underneath the ridges and troughs in the study area exceed the elastic limit of about 10^{-6} m^{-1} and require anelastic failure of the crust.

6. Normal faults are common in sediments on the Tiburon Ridge and south of the Barracuda Ridge [*Peter and Westbrook*, 1976; *Mascle and Moore*, 1990]. Deformed sediments in the Barracuda Trough could be due to either extension or compression [*Roest and Collette*, 1986].

7. Focal mechanisms of 2 large intraplate earthquakes north of the Barracuda Ridge have composite thrust and strike-slip mechanisms [*Bergman*, 1986] and indicate N-S compression.

8. Heat flow on the Tiburon Ridge from Ocean Drilling Program site 672A is 79°C/km [*Fisher and Hounslow*, 1990], about 2.5 times as high as expected on normal ocean crust of this age (about 80 Ma).

9. A 220m thick middle Eocene-upper Oligocene sequence of turbidites was found on the slope of the Tiburon Ridge at Ocean Drilling Program site 672A [*Mascle and Moore*, 1990]. The turbidites are found about 800 m above the adjacent abyssal plain.

These observations and modeling results lead to the following geological interpretation: when transtension started between North America and South America in the Late Cretaceous (we can only calculate this for the time after chron 34 (84 Ma) due to the absence of magnetic anomalies during the Cretaceous Magnetic Quiet Period), the Fifteen-Twenty, Marathon, Mercurius, and Vema fracture zones may have represented structural weaknesses in the oceanic crust. Along their fracture troughs the crust may have been severely thinned already, as has been observed at other fracture zones in the central North and equatorial Atlantic [*Detrick et al.*, 1982, *Sinha and Louden*, 1983, *Morris et. al.*, 1991].

Most likely the transtension localized strain along these structural weaknesses so that the crust was thinned even more. Our analysis of the change in offset through time of the Fifteen-Twenty Fracture Zone versus computed strike slip for the time of transtension (84-67 Ma) suggests that the location of the plate boundary was south of the Fifteen-Twenty Fracture Zone. Hence we would expect to find more evidence for extension in the Tiburon Ridge area than in the Barracuda Ridge/Trough area. This line of reasoning is supported by our crustal model sections from inversion of gravity anomalies, which show more severe thinning under the Tiburon Rise than underneath the Barracuda Ridge.

When the tectonic regime changed to transpression in the Early Tertiary, the deformation caused by compressional stresses may have remained localized at the already thinned crustal areas. This is also likely because of the additional strike slip component of the differential plate motion that may have contributed to lateral motion and faulting of the crust along the fracture zones. Once this process had started a combination of compressional and strike slip components changing throughout the Tertiary may have caused initial crustal buckling that resulted in elastic failure after strain exceeded the linear elastic limit, resulting in runaway deformation as found by *Zuber and Parmentier* [1991]. That strain must have exceeded the elastic limit in the large parts of the area from the Barracuda Trough to south of the Tiburon Ridge is suggested by our map of Moho curvatures exceeding $10^{-6}m^{-1}$ (Figure 14).

Published plate kinematic data cannot resolve the time within the Tertiary when the Barracuda and Tiburon Ridges were uplifted. However, the Eocene-upper Oligocene sequence of turbidites found on the slope of the Tiburon Ridge 800 m above the abyssal plain documents that this ridge must have risen significantly after the Oligocene. The high heat flow on the Tiburon Ridge also fits the scenario well, and may be accounted for by the very shallow Moho (1.5-2 km) underneath the ridge and not by fluid discharge from the nearby accretionary wedge, as suggested by *Fisher and Hounslow* [1990]. The shallow Moho underneath the Tiburon and Barracuda Ridges reflects an unstable density distribution and indicates that compressive stresses may be required at the present time to maintain these anomalies.

CONCLUSIONS

A comparison of fracture zone trends and synthetic flow lines reveals that the North American–South American–African triple junction must have migrated from the Guinea-Demarara shear margin to the to the Vema Fracture Zone before chron 34 (84Ma), to north of the Doldrums Fracture Zone before chron 22 (51.9 Ma), and to north of the Mercurius Fracture Zone between chron 32 (72.5 Ma) and chron 13 (35.5 Ma). Two anomalous ridges on old ocean crust (~84-70 Ma) between the Mercurius and Fifteen-Twenty fracture zones, the Barracuda and Tiburon ridges, exhibit large, short-wavelength Bouguer gravity anomalies (up to 135 mGal), which require mantle densities at shallow levels under the ridges (Moho uplift of up to 4 km). Inversion of Bouguer gravity anomalies for smooth crustal structure yields layers with curvatures exceeding 10^{-6} m^{-1} underneath the ridges and adjacent troughs. This exceeds values permissible under elastic buckling and suggests that this area has been subject to severe deformation as a result of North American-South American plate motions. Plate kinematic data suggest a Late Cretaceous phase of transtension, followed by transpression in the Tertiary for the Tiburon/Barracuda Ridge area. We propose that crustal thinning during the transtensional period was localized at preexisting structural weaknesses such as the Vema, Marathon, and Mercurius fracture zone troughs. A comparison of fracture zones with synthetic flow lines suggests that during most of this period the plate boundary was located between the Vema and the Marathon fracture zones, but may have included the Fifteen-Twenty Fracture Zone after chron 32 (72.5 Ma). This interpretation concurs with our crustal structural model, which shows more severe crustal thinning underneath the Tiburon Ridge than at the Barracuda Ridge. After chron 30 (67 Ma) transtension was replaced by transpression in this area, localizing the resulting strain along the already thinned and weakened crustal sections, creating the ridge/trough topography observed today in the Tiburon/Barracuda Ridge area. Middle Eocene-upper Oligocene turbidites drilled on the flank of the Tiburon Ridge far above the adjacent abyssal plain suggest that much of its uplift has occurred after the Oligocene. High heat flow at the Tiburon Ridge and the unstable density distribution underneath the Tiburon and the Barracuda ridges indicate that uplift due to compressional deformation in this area may still be ongoing today, and that the North American-South American plate boundary may still be located here.

Given this scenario, we would expect to find frequent reverse faults in the plate deformation area. From published seismic sections it appears that normal faults in sediments are more common than reverse faults, but Bull and Scrutton (1992) have interpreted sediment onlap patterns in the Barracuda Ridge area as indicators for rotation and reverse faulting. A combination of seismic reflection and refraction data will be necessary to investigate the style and amount of deformation in this area and compare these data with the North American–South American differential motions and their uncertainties predicted from plate reconstructions.

Acknowledgements. The gridding, contouring, grid sampling, detrending, and graphics software used in this paper comes from the GMT system (*Wessel and Smith*, 1991). Jason Phipps Morgan suggested the smoothing spline inversion approach. The authors would like to thank Andrew D. Walker, Kevin M. Brown, Walter R. Roest, David T. Sandwell, and Christopher Small for many helpful discussions. We thank Hans Schouten and an anonymous reviewer for critical reviews of the manuscript. R.D.M. was supported by a graduate research assistantship and W.H.F.S. by a postdoctoral scholarship from the C.H. and I.M.

Green Foundation for Earth Sciences at the Scripps Institution of Oceanography.

REFERENCES

Backus, G. E., and J. F. Gilbert, Uniqueness in the inversion of gross Earth data, *Phil.os Trans. R. Soc. London, Ser. A, 266*, 123–192, 1970.

Bergman, E.A., Intraplate earthquakes and the state of stress in oceanic lithosphere, *Tectonophysics, 132*, 1-35, 1986.

Bull, J.M., and R.A. Scrutton, Diffuse Plate boundaries in the Indian and Atlantic Oceans,*EOS Trans Amer Geophys Union, 73*, 508-509, 1992.

Cande, S. C., J. L. LaBrecque, and W. F. Haxby, Plate kinematics of the South Atlantic: Chron 34 to present, *J. Geophys. Res., 93*, 13,479–13,492, 1988.

Carlson, R. L., and C. N. Herrick, Densities and porosities in the oceanic crust and their variations with depth and age, *J. Geophys. Res., 95*, 9153–9170, 1990.

Collette, B. J., A. P. Slootweg, J. Verhoef, and W. R. Roest, Geophysical investigations of the floor of the Atlantic Ocean between 10° and 38° N (Kroonvlag-project), *Proc. K. Ned. Akad. Wet., Ser. B, 87*, 1–76, 1984.

Constable, C., and R. Parker, Deconvolution of long-core paleomagnetic measurements–Spline therapy for the linear problem, *Geophys. J. Int., 104*, 453-468, 1991.

Detrick, R. S., M. H. Cormier, R. A. Prince, and D. W. Forsyth, Seismic constraints of the crustal structure within the Vema Fracture Zone, *J. Geophys. Res., 87*, 10,599–10,612, 1982.

Engel, C.G., and R.L. Fisher, Granitic to ultramafic rock complexes of the Indian Ocean ridge system, western Indian Ocean, *Geol. Soc. Am. Bull., 86*, 1553-1578, 1975.

Fisher, A.T., and M.W. Hounslow, Heat flow through the toe of the Barbados accretionary complex, ODP leg 110: Tectonic and hydrologic synthesis, *Proc. Ocean Drill. Program, Sci. Results, 110*, 345-364, 1990.

Karner, G. D., and J. K. Weissel, Factors controlling the location of compressional deformation of oceanic lithosphere in the central Indian Ocean, *J. Geophys. Res., 95*, 19,795–19,810, 1990.

Kent, D. V., and F. M. Gradstein, A Jurassic to Recent chronology, in *The Geology of North America*, vol. M, The *Western North Atlantic Region*, edited by P. R. Vogt and B. E. Tucholke, pp. 45–50, Geological Society of America, Boulder, Colo., 1986.

Klitgord, K. D., and H. Schouten, Plate kinematics of the central North Atlantic, in *The Geology of North America*, vol. M, *The Western North Atlantic Region*, edited by P. R. Vogt and B. E. Tucholke, pp. 351–404, Geological Society of America, Boulder, Colo., 1986.

Mascle, A., and J.C. Moore, ODP leg 110: Tectonic and hydrologic synthesis, *Proc. Ocean Drill. Program, Sci. Results, 110*, 409-424, 1990.

Mascle, J., E. Blarez, and M. Marinho, The shallow structures of the Guinea and Ivory Coast-Ghana transform margins: Their bearing on the equatorial Atlantic Mesozoic evolution, *Tectonophysics, 155*, 193–210, 1988.

Mauffret, A., G. K. Westbrook, M. Truchan, and J. Ladd, The relief of the oceanic basement and the structure of the front of the accretionary complex in the region of sites 541, 542 and 543, *Initial Rep. DSDP, 78A*, 49–56, 1984.

McKenzie, D., and C. Bowin, The relationship between bathymetry and gravity in the Atlantic Ocean, *J. Geophys. Res., 81*, 1903–1915, 1976.

McNutt, M. K., Lithospheric flexure and thermal anomalies, *J. Geophys. Res., 89*, 11,180–11,194, 1984.

Menke, W., *Geophysical Data Analysis: Discrete Inverse Theory*, 2nd rev. ed., 285 pp., Academic, San Diego, Calif., 1989.

Morris, E., R. S. Detrick, T. A. Minschull, R. S. White, P. Buhl, and J. C. Mutter, Variations in crustal structure: Normal vs. fracture zone crust, *EoS Trans. AGU, 72*, 431, 1991.

Mulder, T. F. A., and B. J. Collette, Gravity anomalies over inactive fracture zones in the central North Atlantic, *Mar. Geophys. Res., 6*, 383–394, 1984.

Müller, R. D. and W. R. Roest, Fracture zones in the North Atlantic from combined Geosat and Seasat data, *J. Geophys. Res., 97*, 3337-3350 1992.

Müller, R.D., D.T. Sandwell, B.E. Tucholke, J.G. Sclater, and P.R. Shaw, Depth to basement and geoid expression of the Kane Fracture Zone: A comparison, *Mar. Geophys. Res., 13*, 105-129, 1991.

Oldenburg, D.W., The inversion and interpretation of gravity anomalies, *Geophysics, 39*, 526-536, 1974.

Parker, R. L., The rapid calculation of potential anomalies, *Geophys. J. R. Astron. Soc., 31*, 447–455, 1972.

Peter, G., and G.K. Westbrook, Tectonics of southwestern North Atlantic and Barbados Ridge complex, *Am. Assoc. Pet. Geol. Bull., 60*, 1078-1106, 1976.

Purdy, G. M., The seismic structure of 140 my old crust in the western central Atlantic Ocean, *Geophys. J. R. Astron. Soc., 72*, 115–137, 1983.

Roest, W. R., Seafloor spreading pattern of the North Atlantic between 10° and 40°N, *Geol. Ultraiectina, 48*, 121 pp., 1987.

Roest, W. R., and B. J. Collette, The Fifteen Twenty Fracture Zone and the North American-South American plate boundary, *J. Geol. Soc. London, 143*, 833–843, 1986.

Sandwell, D.T. and W.H.F. Smith, Global marine gravity from ERS-1, Geosat and Seasat reveals new tectonic fabric, *EoS Trans. AGU, 73*, 133, 1992.

Shaw, P. R., and S. C. Cande, High-resolution inversion for South Atlantic plate kinematics using joint altimeter and magnetic anomaly data, *J. Geophys. Res., 95*, 2625–2644, 1990.

Sinha, M. C., and K. E. Louden, The Oceanographer Fracture Zone – I. Crustal structure from seismic refraction studies, *Geophys. J. R. Astron. Soc., 75*, 713–736, 1983.

Smith, W. H. F., On the accuracy of digital bathymetric data, *Jour. Geophys. Res.*, in press, 1993.

Smith, W. H. F., and P. Wessel, Gridding with continuous curvature splines in tension, *Geophysics, 55*, 293–305, 1990.

Tucholke, B. E., R. E. Houtz, and W. J. Ludwig, Sediment thickness and depth to basement in western North Atlantic Ocean basin, *AAPG Bull, 66*, 1384–1395, 1982.

Tucholke, B.E. and H. Schouten, Kane Fracture Zone, *Mar. Geophys. Res., 10*, 1-39, 1988.

Watts, A. B., An analysis of isostasy in the world's oceans, 1, Hawaiian-Emperor seamount chain, *J. Geophys. Res., 83*, 5989–6004, 1978.

Wessel, P. and W.F. Haxby, Thermal stresses, differential subsidence, and flexure at oceanic fracture zones, *J. Geophys. Res., 95*, 375-391, 1990.

Wessel, P. and W. H. F. Smith, Free software helps map and display data, *EoS Trans. AGU, 72*, 445, 1991.

Wessel, P., and A. B. Watts, On the accuracy of marine gravity measurements, *J. Geophys. Res., 93*, 393–413, 1988.

Westbrook, G. K., A. Mascle, and B. Biju-Duval, Geophysics and the structure of the Lesser Antilles Arc, Initial Rep. DSDP, *78A*, Washington, 23–38, 1984.

Zuber, M. T., and E. M. Parmentier, Fold growth in a non-Newtonian viscous lithosphere: Implications for horizontal shortening associated with intraplate folds in Indian Ocean seafloor, *EoS Trans. Amer. Geophys. Union, 72*, 472, 1991.

R.D. Müller, SIO, UCSD, 9500 Gilman Dr., La Jolla, CA 92093-0208.

W.H.F. Smith, Geosciences Laboratory, Ocean and Earth Sciences, NOS, NOAA, 11400 Rockville Pike, Rockville, MD 20852.

(Received January 10, 1992;
revised September 21, 1992;
accepted December 4, 1992.)